30 e

MAGNETIC MOMENTS IN AMORPHOUS PALLADIUM-COBALT-SILICON ALLOYS

Thesis by

Martin Eric Weiner

In Partial Fulfillment of the Requirements

For the Degree of

Doctor of Philosophy

California Institute of Technology

Pasadena, California

1968

(Submitted May 15, 1968)

ACKNOWLEDGMENTS

I would like to thank Dr. Pol Duwez for his encouragement, suggestions, and personal interest in this work. Dr. R. H. Willens served as my research advisor for the year 1965-1966 and I would like to thank him for his help in the construction of the magnetometer, his design of the variable temperature chamber, and his continued interest in my work after leaving Caltech. Gary Nix was responsible for the design and construction of the automatic temperature controller described in this thesis and assisted in taking experimental data.

I would like to express my appreciation to the U. S. Atomic Energy Commission for their financial support and the U. S. National Science Foundation and the U. S. Steel Corporation for Fellowship aid.

ABSTRACT

The magnetic moments of amorphous ternary alloys containing Pd, Co and Si in atomic concentrations corresponding to $Pd_{80-x}Co_xSi_{20}$ in which x is 3, 5, 7, 9, 10 and 11, have been measured between 1.8 and 300°K and in magnetic fields up to 8.35 kOe. The alloys were obtained by rapid quenching of a liquid droplet and their structures were analyzed by X-ray diffraction. The measurements were made in a null-coil pendulum magnetometer in which the temperature could be varied continuously without immersing the sample in a cryogenic liquid. The alloys containing 9 at.% Co or less obeyed Curie's Law over certain temperature ranges, and had negligible permanent moments at room temperature. Those containing 10 and 11 at.% Co followed Curie's Law only above approximately 200°K and had significant permanent moments at room temperature. For all alloys, the moments calculated from Curie's Law were too high to be accounted for by the moments of individual Co atoms. To explain these findings, a model based on the existence of superparamagnetic clustering is proposed. The cluster sizes calculated from the model are consistent with the rapid onset of ferromagnetism in the alloys containing 10 and 11 at.% Co and with the magnetic moments in an alloy containing 7 at.% Co heat treated in such a manner as to contain a small amount of a crystalline phase. In alloys containing 7 at.% Co or less, a maximum in the magnetization vs temperature curve was observed around 10°K. This maximum was eliminated by cooling the alloy in a magnetic field, and an explanation for this observation is suggested.

TABLE OF CONTENTS

I. INTRODUCTION

The existence of ferromagnetism in amorphous solids has been predicted theoretically. In the model used by Gubanov,[1] there is no long range periodic arrangement of atoms in a lattice, and only the exchange integral of neighboring ferromagnetic atoms and the radial distribution function of the structure are taken into consideration. Ferromagnetic amorphous alloys have been obtained by two different techniques. By evaporating cobalt and gold on a substrate at liquid nitrogen temperature, Mader and Nowick[2] succeeded in depositing amorphous films as thick as about 600 A. The films containing from 25 to 60 at.% Co were ferromagnetic. By rapid quenching from the liquid state, Tsuei and Duwez[3] obtained amorphous ferromagnetic alloys containing 68 at.% Pd, 12 at.% Co and 20 at.% Si.

This particular alloy has a remanence of about 0.1 G and a coercive force of 466 Oe. As explained in Ref. (3), the ternary Pd_{68}-Co_{12}-Si_{20} amorphous alloy is just one of a series of amorphous alloys whose compositions can be represented by Pd_{80-x}-F_x-Si_{20} in which F represents any of the three ferromagnetic elements Fe, Co, or Ni, and x is the concentration of that element. The maximum values of x beyond which the amorphous structure cannot be obtained are approximately 5 at.% Fe, 12 at.% Co and 15 at.% Ni. When no ferromagnetic element is present, the binary amorphous alloy Pd_{80}-Si_{20} is diamagnetic. The main purpose of the present investigation was to study the formation of localized magnetic moments in the ternary Pd-Co-Si alloys as a function of cobalt content.

II. EXPERIMENTAL PROCEDURES

A. Alloy Preparation and Structure Determination

The ternary palladium-cobalt-silicon alloys were prepared by induction melting. The three elements were of the following purities: 99.99% pure Pd from Engelhard Industries; spectrographic quality Co from Johnson and Matthey containing 10 ppm Si, 5 ppm Ni, 2 ppm Fe and less than 2 ppm of other metallic impurities; transistor grade silicon of at least 99.999% purity. As explained in Ref. (4), a strong exothermic reaction takes place between Pd and Si and no reaction occurs between the melt and the fused silica crucible. Since the weight losses after melting were always less than 0.2%, no chemical analyses were performed and all alloy compositions reported are the nominal ones.

The amorphous structure in the Pd-Co-Si alloys was obtained by rapid quenching from the liquid state. The "piston and anvil"technique described in Ref. (5) was used because rather large specimens (about 50 microns in thickness and 20 or more mm in diameter) can be obtained. In their present state of development, the techniques for rapid quenching from the liquid state do not always yield reproducible results because, as explained in Ref. (5), the actual rate of cooling can vary within large limits from specimen to specimen. As a result of these shortcomings it is necessary to study the structure of every one of the quenched specimens before proceeding with the measurements of their physical properties. In the present study, the structure of the

quenched alloys should be "amorphous", the term amorphous being taken in the sense that the atomic arrangement in the solid, as determined by various techniques such as X-ray diffraction, electron diffraction and electron microscopy is similar to that found in liquid alloys or in solids generally classified as glasses. The X-ray diffraction pattern of an amorphous Pd-Co-Si alloy is practically identical with that of an amorphous binary Pd_{80}-Si_{20} alloy described in Ref. (5). It consists of four or five very broad maxima and the analysis of such a pattern leads to a radial distribution function very similar to that found for liquid structures.[5] After many years of experience in quenching liquid alloys into an amorphous structure, it has been found that when the quenching conditions are not the optimum ones, the X-ray diffraction pattern of the quenched foil still shows the same very broad peaks, but a few weak but sharp Bragg reflections are present. This means that most of the foil still consists of an amorphous phase, but isolated crystals of an equilibrium (or in some cases a non-equilibrium)phase are present. The existence of this type of duplex structure in quenched foils has been described in Ref. (5). Experience has also shown that if a quenched foil contains a small amount of a crystalline phase, this phase is likely to generate a sharp peak at a Bragg angle located near the maximum of the first very broad amorphous diffraction band. The presence of weak Bragg reflections superimposed on the broad maximum due to the amorphous band cannot be detected by the usual diffractometer scanning using a rate meter since weak diffraction peaks would be lost

within the noise limits. An X-ray diffraction pattern of each foil studied in this investigation was therefore taken with a diffractometer equipped with a step-scanning mechanism so that intensity measurements could be taken with a statistical accuracy of about 0.6% in steps of 0.05^{o} in 2θ within the critical range of Bragg angles between 30 and 50^{o} in 2θ. The total time required for a full scanning of an amorphous specimen was about 10 hours. This time was of course much shorter for specimens for which a Bragg peak appeared on the diffraction pattern during scanning.

During the course of this investigation it became advisable to measure magnetic moments in alloys containing very small amounts of a crystalline phase. Since the kinetics of crystallization of amorphous Pd-Co-Si alloys is not known, a few preliminary experiments were necessary to determine what heat treatment would lead to the onset of crystallization. Amorphous foils were sealed in evacuated pyrex tubes and heated for various lengths of time at 250, 300 and $325^{o}C$. After ageing at $325^{o}C$ for 96 hours, weak Bragg reflections were observed in the X-ray diffraction pattern obtained by step scanning. A comparison between the diffraction patterns of the amorphous and the partly crystallized specimens is shown in Fig. 1. The weak crystalline peaks superimposed on the amorphous band are characteristic of one of several either stable or metastable crystalline phases but their complete identification would require a long and tedious study of crystallization kinetics. Since the main purpose of these experiments was to find out the effect

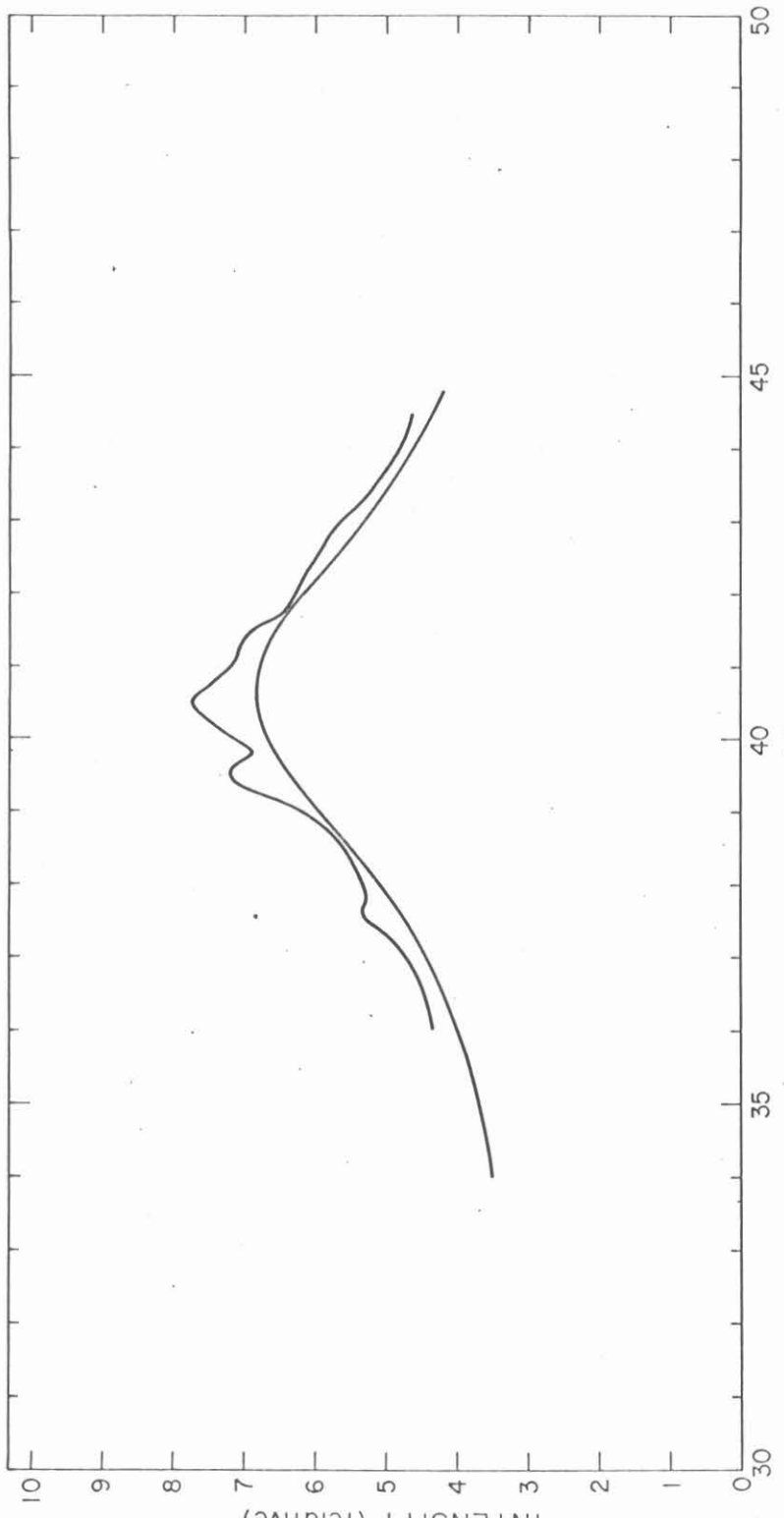

Fig. 1. X-ray diffraction patterns of amorphous (lower, smooth curve) and partly crystallized alloys containing 7 at.% Co.

of the presence of a small amount of crystalline phases on the magnetic moments, a precise knowledge of the crystal structure of these phases was not required for interpreting the results.

B. Design and Performances of the Magnetometer

A wide variety of techniques have been employed for the measurement of magnetic moments. For metals, the most commonly used type of magnetometer involves the measurement of the force exerted on a sample located in a magnetic field. One may either measure the force directly or one can use a null technique in which the force is counterbalanced by inducing a magnetic moment in a coil located in the same field as the sample. The null condition is that the magnetic moment of the coil be equal in magnitude but opposite in sign to that of the sample.

Force magnetometers may be divided into two main groups. One consists of those in which the magnetic force is vertical (balance type) and the other of those in which it is horizontal (pendulum type).

One common balance type magnetometer was described by W. Sucksmith.[6],[7] He employed a rigid rod attached to a ring which deflected under the application of a vertical load. Two mirrors were mounted on the ring at positions calculated to give maximum deflection to a light beam intercepting both mirrors. The deflection was read by a travelling microscope and calibrated by applying a known weight to the base of the ring. His electromagnet had pole pieces tapered for constant $H \frac{dH}{dX}$ for paramagnetic samples and $\frac{dH}{dX}$ for ferromagnetic ones. His method necessitates a guiding device to prevent lateral motion of the

rigid rod. Many other balance type magnetometers have been described, the basic difference among them being the force measuring device. Lundquist and Myers[8] described a strain gage measuring system. Soule, et al.[9] used a quartz beam microbalance and a null technique. In the latter, the beam was counterbalanced with a magnetic rod, and a solenoid was used to increase or decrease the effective mass of the counterweight to achieve a null.

Pendulum magnetometers have been described by Bozorth, et al.[10] and Jongenburger and Berghout.[11] Both employed a null technique with compensation accomplished by passing current through a coil rigidly attached to the pendulum at a position such that it was affected by the same field as the sample. Then under certain conditions described by Jongenburger and Berghout, the moment induced in the coil will equal that in the sample (apart from a difference in sign). In particular, $\frac{dH}{dX}$ should be constant over the entire coil. Bozorth, et al. used strain gages for null detection and Jongenburger and Berghout used a differential transformer. In an updating of the apparatus used by Bozorth, et al., Sherwood[12] described the use of silicon strain gages and suggested a technique for aligning the pendulum in the field with an accuracy of the order of $\pm$ 0.1 degree. This is particularly important in studies of anisotropy.

In comparison with other methods, force magnetometers have a number of advantages. First of all, the moment measured is completely independent of the geometry of the sample (except for demagnetizing fields). They are particularly desirable for measurements in metals

since a d.c. field is used and no eddy current problem arises. Perhaps most significant is that they directly measure the force on a sample located in a magnetic field. Thus there is no ambiguity in the results if the measurements are carried out properly. One disadvantage of the force method is that the force depends on the field applied and sensitivity is very low for small fields. Another disadvantage common to any technique involving mechanical motion is the sensitivity to vibration and convection currents.

The major advantage of the pendulum type magnetometer over the balance type is the fact that the gravitational force is perpendicular to the magnetic force. Since the latter is typically much smaller than the weight of the moving section of the magnetometer, the balance type involves the measurement of a small change in force at a high absolute level. In addition, the moving section of the magnetometer is normally suspended in a small tube. Thus, any temperature gradient would tend to create vertical convection currents, affecting a balance system more than a pendulum system. This effect could be very serious near the temperature of liquid helium, where a small change in temperature corresponds to a large change in pressure. A further advantage lies in measurements on strongly ferromagnetic materials, which tend to be attracted toward one of the pole pieces of the magnet. A pendulum can be constrained to a single axis of motion without any friction devices.

The magnetometer used for this investigation is of the horizontal type using the null method. An electrical detecting system was decided upon because it is capable of a wide range of sensitivities and permits

the use of phase sensitive detection. Strain gages were used because of their simplicity and compactness and because the bending beam to which they are bonded provides a natural damping action. Furthermore, the development of low temperature coefficient silicon strain gages[13] enables measurements of much lower strains than metal gages. A counterweight system was designed to overcome both the restoring torque of the bending beam and the effect of gravity to any extent desired. An analysis of the entire strain gage-pendulum system is given in appendix A.1.

The basic features desired in the construction of the magnetometer were:

1. Control of the temperature of the strain gages as well as other critical electrical components.
2. Protection of the strain gages during assembly and during changing of the sample.
3. Easy assembly and disassembly of various parts.
4. Minimum pendulum mass.
5. Minimum magnetic moment of the components in the magnetic field.
6. The use of an exchange gas to avoid immersing the pendulum in a liquid, especially at its boiling point.
7. A system for continuous temperature control from $1.3^{\circ}K$ to $300^{\circ}K$.
8. Ability to adapt to a slightly modified standard Select-a-Stat dewar manufactured by Sulfrian Cryogenics. The tail section

of this model is demountable and one constructed in the standard three wall fashion with a 1 1/2" outer diameter was used.

The problems involved in the construction of the pendulum support (see Fig. 2) were to provide a heat path to the strain gages for temperature control, to align the strain gage spring both vertically and with the magnet, and to allow small final adjustments to insure free motion of the pendulum. The support was machined out of two pieces of copper. The lower part was machined first and all dimensions were measured accurately to insure proper alignment and correct pendulum length. The slot milled for the strain gage spring was used as an alignment reference. Then the upper part was machined, except for the bolt holes, and silver brazed to the lower part with care taken to avoid distortion. After brazing, eight oversized bolt holes were drilled using a dividing head chuck with the centers of one pair of holes in the same plane as the strain gage spring. The oversized holes allow the small lateral adjustments mentioned above. A spiral arrangement of 1/4" Cu tubing was soft soldered to the top of the pendulum support as part of the water temperature control system (see Appendix A.2). To insure proper vertical alignment of the pendulum, pieces of drill rod were pressed into two of the holes in the strain gage spring groove and the third was tapped to allow fastening. This method of fastening permits good thermal contact between the spring and the pendulum support as well as easy disassembly. The wires from the two strain gages and the pendulum coil were

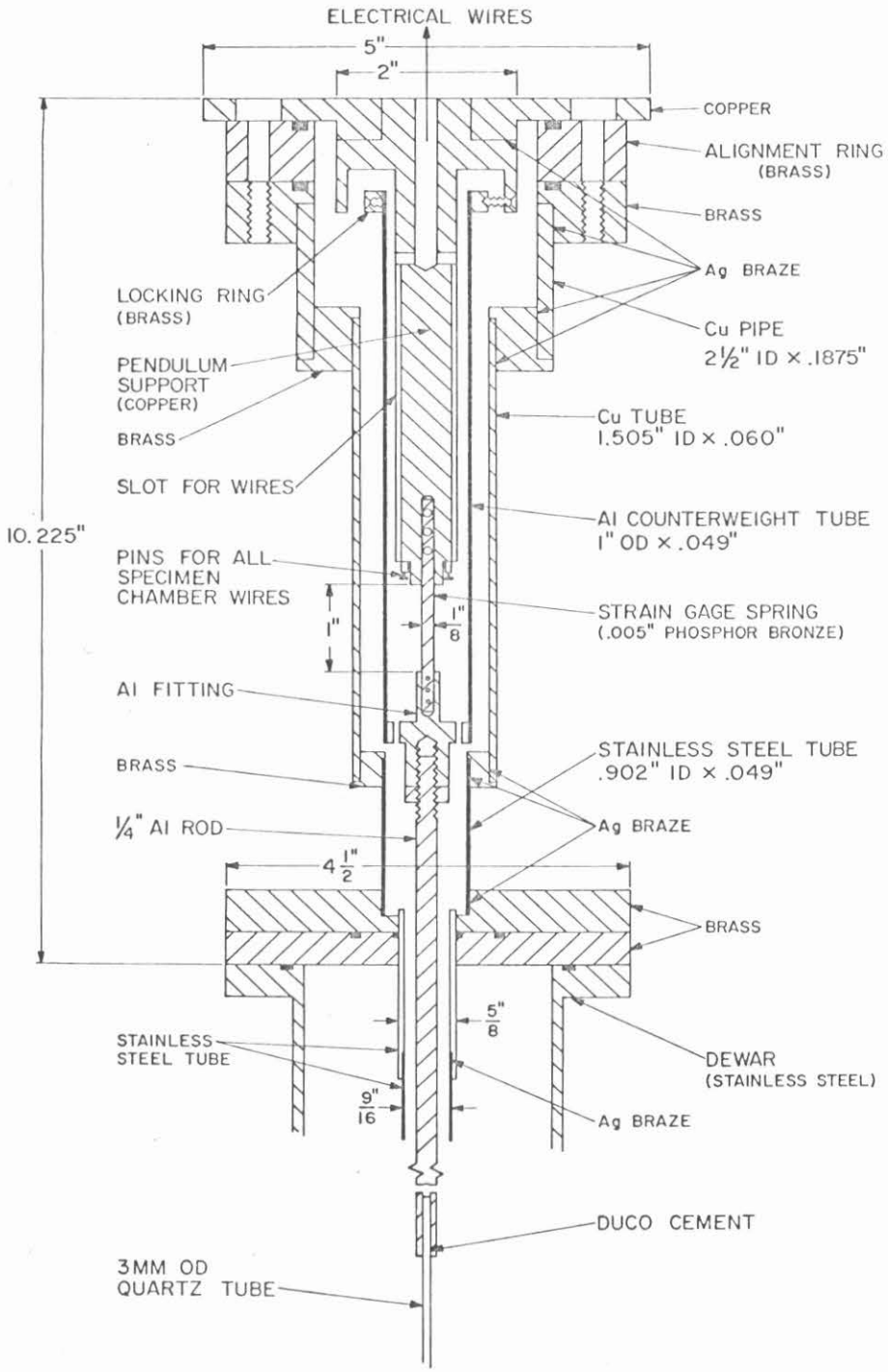

Fig. 2. Drawing of upper section of Pendulum, Pendulum Support, and Upper Specimen Chamber.

soldered to terminals near the top of the strip. Wires from the terminals then lead through grooves in the pendulum support to a center hole and into a vacuum-tight connector box (see Fig. 3). These terminals assist in easy assembly and disassembly of the components of the pendulum.

The strain gage spring was machined from a piece of 0.005" thick phosphor bronze which was glued to a flat piece of aluminum with duco cement. After machining, the springs were easily removed with acetone. The silicon strain gages were bonded to one of the springs by the manufacturer. (Microsystems, Inc., Pasadena, California).

At the bottom of the spring is an aluminum fitting, machined from a single piece of aluminum. The spring was attached to and aligned with the fittings using the technique previously described for the copper pendulum support. The counterweight tube was attached to this fitting with three screws, allowing easy access to the strain gages and electrical connections.(see Figs. 2 and 3).

The next member of the pendulum assembly is an aluminum rod which is screwed into the aluminum fitting. It is locked in place with an aluminum nut and a lock washer. The bottom of the rod was drilled out to accommodate the quartz tube with a minimum of clearance. This was necessary to insure vertical alignment of the pendulum. Quartz was used for the remainder of the pendulum because of its high modulus (relative to other nonmetallic materials), low thermal conductivity, and extremely low thermal expansion. The last of these is particularly

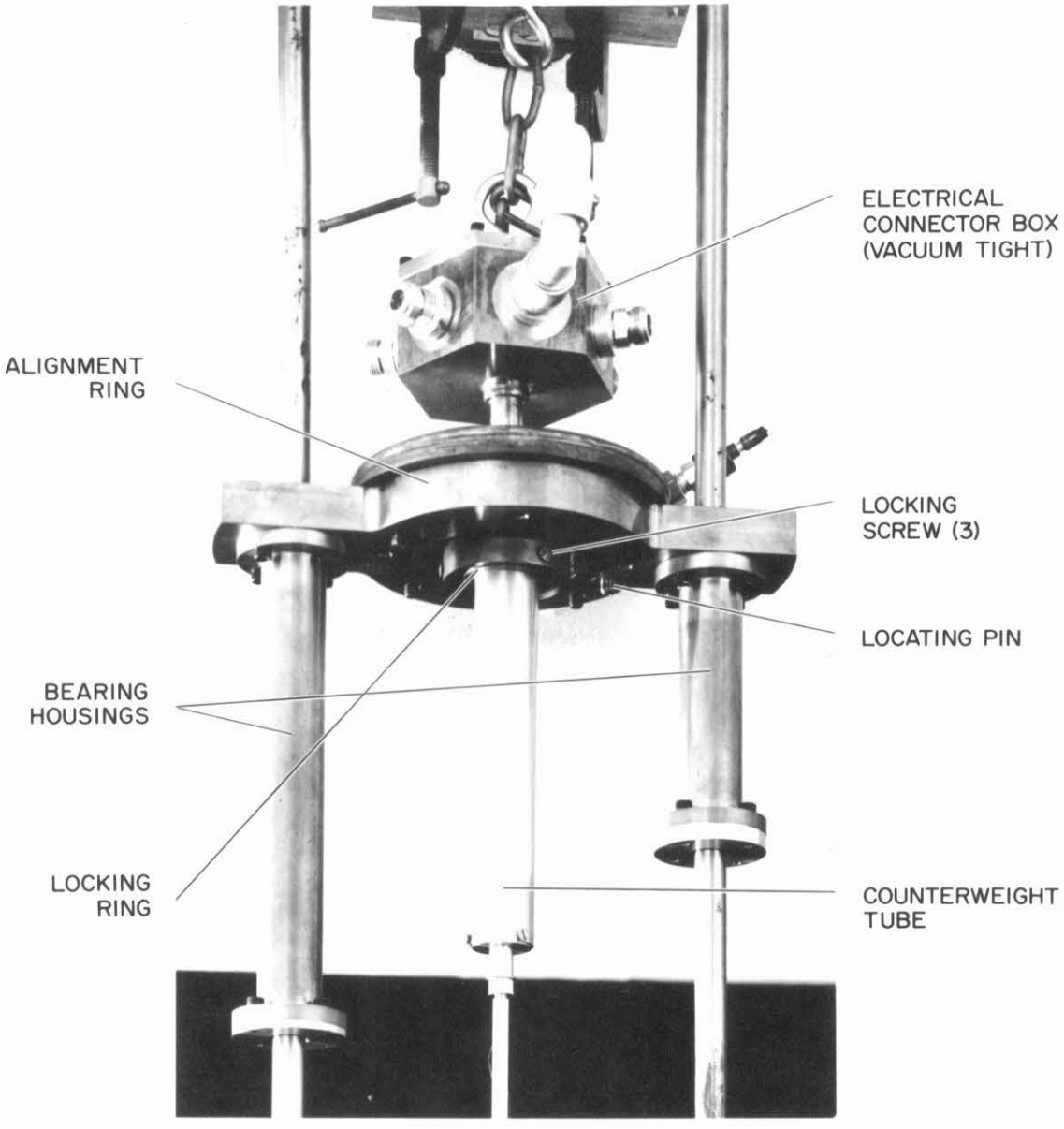

Fig. 3. Pendulum Support and Related Equipment.

desirable since the position of the null-coil (and sample) in the field is then independent of temperature. The quartz tube was glued in place with duco cement (easily dissolved) and the wires were brought out through side holes as in Fig. 2. The quartz tube was attached to a quartz coil form (see Fig. 4) and the coil wound by hand afterward. The latter consists of about 100 turns of 32 gage nyclad copper magnet wire. Each layer was coated with G.E. No. 7031 insulating varnish. This varnish performs quite well in vacuum and at low temperatures. The center of the quartz tube was used as a guide for the wires. Thus, one may have several quartz tubes available - e.g., for various ranges of magnetic moment or different sample sizes - and install them in a short time with minimum disassembly. If the tubes are quite straight and care is taken in aligning the axis of the coil with the axis of the magnet and with the strain gage spring, only a minimum of adjustment is necessary. Each tube must be recalibrated every time it is reinstalled in the instrument.

The counterweight tube was made from standard size aluminum tubing (the aluminum fitting to which it was attached was designed to accommodate it). A lathe was employed to obtain the correct length and to square the ends. The three screw holes were drilled in a milling machine using a dividing head chuck.

A locking ring was designed to protect the strain gages. It was machined from a piece of 1 1/2" brass rod. It contains three set screw holes and three countersunk holes to accommodate the locking screws

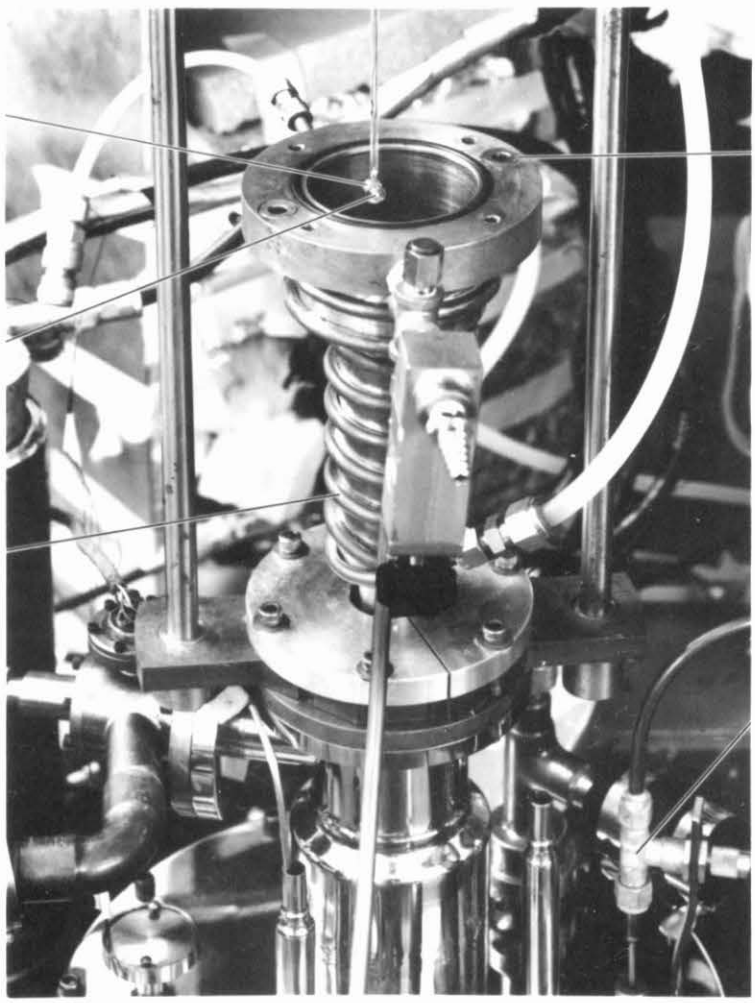

Fig. 4. Upper Specimen Chamber and Pendulum Coil.

(see Figs. 2 and 3). All six holes were drilled using a dividing head chuck to insure uniform distribution of mass and proper alignment for the locking screws. The locking screws were machined to the correct length and their tips, to the correct conical shape. This insures that the pendulum is still vertical in the locked condition. A counterweight could have been installed in a fashion similar to the locking ring, since the specimen chamber was designed to accommodate such a counterweight. However, the center of mass of the first pendulum constructed was quite close to the bottom of the strain gage spring and no counterweight was needed to obtain good sensitivity.

The alignment ring (see Figs. 2 and 3) was designed to insure alignment of the pendulum after each specimen change. It was machined from 3/4" thick flat brass to a 9" diameter. Then eight holes concentric with those on the top of the pendulum support were drilled in it. Four of these were tapped to allow the pendulum support to be attached to it and four were drilled to allow bolts to pass through. During final assembly the pendulum was adjusted as mentioned above and bolted tightly to the alignment ring. The alignment ring and pendulum support then effectively became a single unit. This combination was then fastened with four bolts to the specimen chamber flange. In order to obtain precise alignment after a change of specimen, there are case-hardened locating pins in the alignment ring and matching liners in the specimen chamber flange. These insure position repeatability within 0.0007", which is well beyond that required. To facilitate changing of

samples, two housings containing linear ball bearings were attached to the alignment ring. These guide the pendulum assembly along two case-hardened 1/2" steel rods (see Fig. 5). To avoid tilting, there are two bearings on one side to allow three-point support. Much of the mass of the alignment ring served no purpose after machining and was milled away in order to lower the weight supported by the dewar.

The upper flange of the specimen chamber (see Fig. 2) was machined from 3/4" flat brass. Four holes were drilled and tapped in it to allow fastening of the pendulum support - alignment ring assembly. The rest of the upper section of the chamber was made up of standard tubes and pipes, as indicated in Fig. 2. These were cut to the proper length and the two brass reducing fittings were machined from pieces of brass rod. The lower flange of the upper section was made from 1/2" flat brass. A disc, 8 1/2" in diameter, was first machined. Then holes for six bolts and for the two lower support fittings for the steel guide rods (see Fig. 5) were drilled. Next, all excess material was milled away. The entire assembly was then silver brazed and checked on a lathe for concentricity. Soft copper tubing, 1/4" in diameter, was wound around the copper parts of the specimen chamber and soft soldered to it. This assembly constitutes a part of the temperature control system for the electrical components (see Appendix A.2). In order to allow raising of the pendulum, quick-disconnect couplings were installed in the water lines of the temperature control system where necessary.

The lower part of the specimen chamber consists of a variable

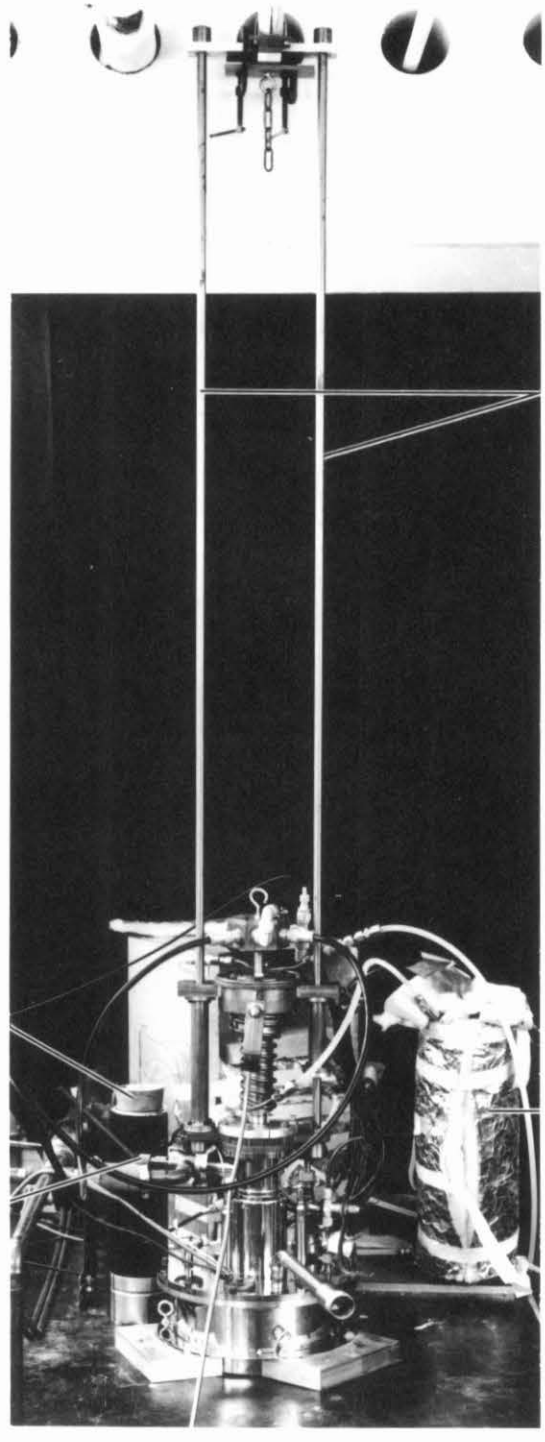

Fig. 5. Magnetometer in Closed (Operating) Position.

temperature chamber and a connecting tube (see Fig. 6). In order to insure a vacuum-tight seal between the connecting tube and the dewar, a 3/8" brass disc with two O-ring grooves and a center hole to allow the connecting tube to pass through was machined and positioned above the neck of the dewar (see Fig. 2). It has six bolt holes aligned with those on the dewar flange. Since the neck is not available for filling the cryogenic storage chamber, the dewar was modified by the manufacturer to allow transfer through a separate bayonet coupling.

The connecting tube mentioned above actually consists of several sections joined by silver brazing. There is a thick-walled stainless steel section at the top to allow for an O-ring seal and two thin-walled sections joined by a stainless steel bellows. This arrangement provides minimal heat transfer and allows for thermal expansion. There are two sections of copper wool attached to brass rings which were in turn soft soldered to the thin-walled stainless steel tube. These lower the amount of radiative heat transfer to the cryogenic bath and minimize the temperature gradient in the lower part of the specimen chamber.

The variable temperature chamber is shown in Fig. 6. The section containing the double thread was machined from a rod of OFHC copper. The sides of the lower part of the copper section were machined flat to allow room for the grooves joining the two threads and to maximize the space available for the pendulum coil. The coil must swing parallel to these flat sides and the alignment problem was solved by marking the dewar and orienting it before matching the holes on the bottom of the

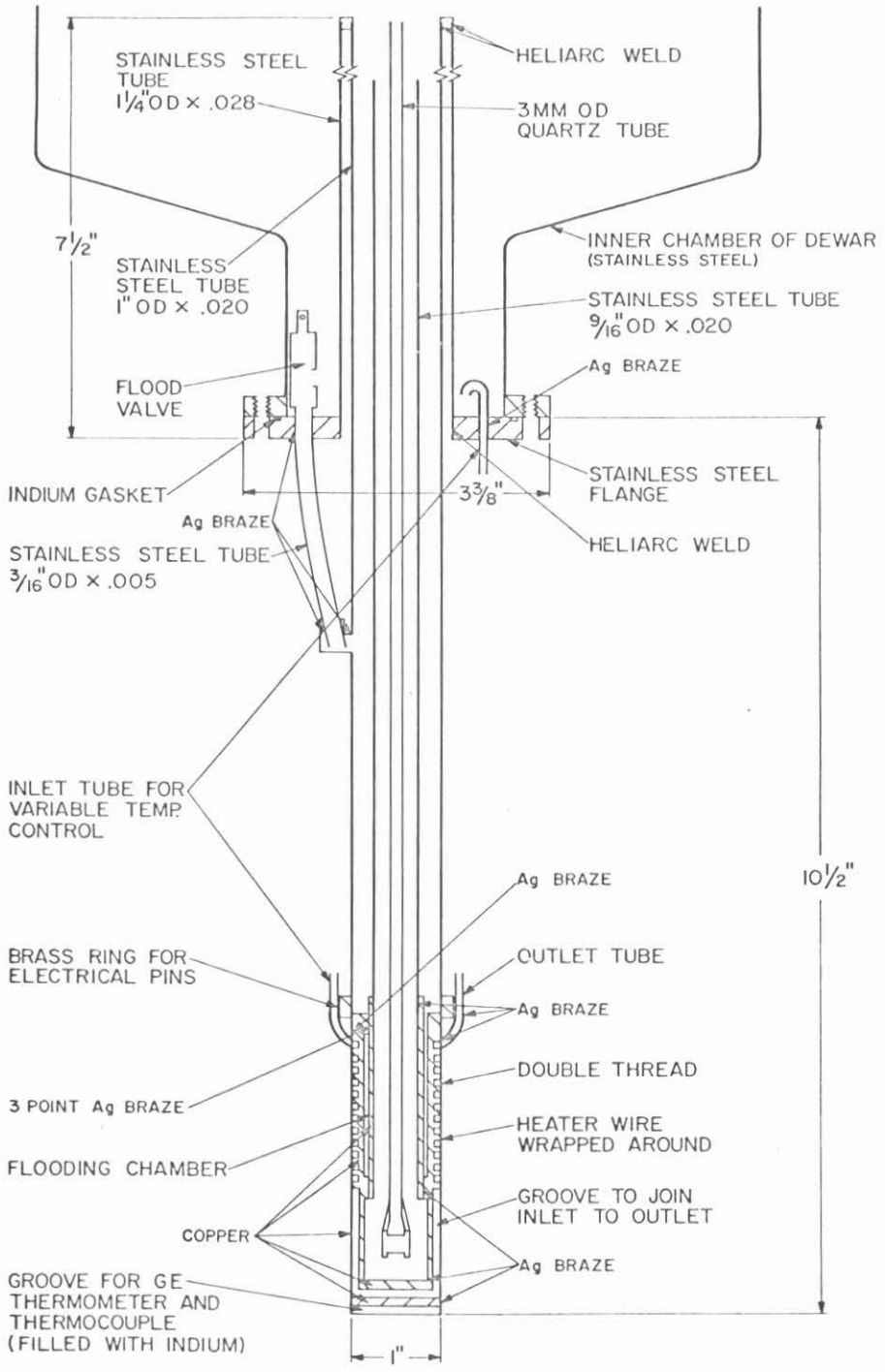

Fig. 6. Drawing of Lower Section of Pendulum and Lower Specimen Chamber (Variable Temperature Chamber).

upper part of the specimen chamber to those in the dewar flange. Thus, in the final assembly, the strain gage spring, the pendulum coil, and the variable temperature chamber are simultaneously aligned with the magnet. After machining of the OFHC copper rod was completed it was lightly pressed into a thin-walled copper tube. Since slight mixing of the inlet and outlet gases (see below) does not pose a problem, there is no seal between the inlet and outlet threads. Then the various welds and brazes indicated in Fig. 6 were made. The next step was to check concentricity on a lathe and to check for leaks in the various sections. The latter was done with a mass spectrometer leak detector sensitive to helium. The entire assembly was then installed in the dewar (before installation of the upper section of the specimen chamber) and held in place with 12 bolts via the stainless steel flange shown in Fig. 6. The necessary vacuum seal was made with an indium gasket. Both the inlet and outlet tubes shown in Fig. 6 follow a spiral path around the specimen chamber above the variable temperature section. The outlet tube was wrapped around and soft soldered to the stainless steel connecting tube just below the flange in order to lower the temperature gradient in the specimen chamber. It then leads through a vacuum-tight coupling on top of the dewar to a needle valve used to control the gas flow. (see Fig. 4).

In operation, there are two techniques for controlling the temperature of the variable temperature chamber. One method is to open the flood valve and to allow the cryogen to flow down into the flooding

chamber. The valve is operated by pulling on a wire which passes through the pump-out port of the dewar. It is a standard spring-loaded toggle valve which was machined to allow it to fit in the small space available and fitted with a teflon seat. At the top, the wire is attached to a piece of drill rod which slides through a vacuum tight coupling. A stainless steel tube was bent and positioned to guide the wire around the 90^{o} turn from the neck of the dewar to the pump-out port (see Figs. 5 and 6). Temperature control employing this valve is used for measurements at a boiling point, measurements below $4.2^{o}K$, and to aid in lowering the temperature from one measuring point to the next. The second method for controlling temperature is used for all other temperatures desired. In this method, a balance between a flow of gas through the double thread and current through a heater is used. The heater current is supplied by an automatic temperature controller (see Appendix A.4). The gas flow is achieved by applying slight pressure to the cryogenic bath (normally only a 1 1/2 psi safety release valve is used) and opening the needle valve mentioned above. The heater consists of several turns of constantan wire wrapped around the variable temperature chamber. As in the case of the pendulum coil, G.E. No. 7031 insulating varnish was used. Measurement of temperature is discussed in Appendix A.4.

In order to measure the level of cryogen in the inner chamber of the dewar and of the liquid nitrogen in the chamber used for radiation shielding, two three-position carbon resistor level indicators were

constructed. The resistors had a nominal value of 300Ω and were attached to thin-walled stainless steel tubing. Two 1 1/2 volt batteries are used as a source of power and the current through the resistors determines the level of the liquid. In liquid nitrogen, the current through a resistor is about 7.2 ma and in liquid helium, 0.8 ma. If the cryogen is not boiling too rapidly, the value of the current in each case increases about 0.5 ma if the resistor is slightly above it.

After assembly of the various components of the system, several problems remained before making measurements. First of all it was necessary to check for noise in the electronics. This is discussed in Appendix A.2. Next, it was necessary to align the pendulum. Since the magnetometer was not intended for experiments involving directionally dependent magnetic moments, it was not considered necessary to attempt a rotational alignment better than that achieved during assembly. However, some lateral adjustment and slight tilting of the dewar were necessary to obtain free motion of the pendulum. To check the swing, an impulse was given to the pendulum by turning the current to the pendulum coil on and off while the electromagnet was on. Then the detector signal prior to the variable time constant filter of the lock-in amplifier (see Appendix A.2.) was observed on an oscilloscope. When an adjustment position was found such that the signal appeared as a clean sinusoidal one, it was assumed that the pendulum was free of constraint. Additional evidence for proper alignment of the pendulum was obtained by observing that the detector signal followed the gradual application

of a small field smoothly in both directions, and by making sure that the pendulum returned to the same position after removal of the field.

After alignment, it was necessary to determine the coil current required to overcome the moment of the section of the pendulum in the field. Since samples whose moments are to be measured are wrapped in a piece of Al foil, a piece of about the right mass (7 mg) was inserted into the coil for the determination of this correction current. This null correction was measured as a function of field and temperature over the range of operation of the magnetometer. The correction was found to be negligible except below 10^{o}K or for measurements on samples with small moments. The moment of impurity iron in the copper wire forming the pendulum coil was assumed responsible for most of the correction below 20^{o}K. The effect of the Al foil was checked at several temperatures and found to be negligible for most measurements. The pieces used were always cut from the same lot and matched within 0.5 mg. The maximum total correction is 2×10^{-3} emu and does not seriously affect most measurements. For samples where one wishes to use the maximum sensitivity available in the magnetometer, it would be wise to make a separate check of the correction current with the same piece of Al foil to be used with the sample. Both the field and the temperature should be reproduced accurately during the measurement on the sample.

The pendulum coil was calibrated by using a piece of high purity Ni foil. The Ni was supplied by Johnson, Matthey & Co., Limited. Their

spectrographic analysis showed 8 parts per million of Fe, 3 ppm of Si and less than 1 ppm of all other elements. The nickel was sealed in an evacuated quartz tube and annealed at 1200°C for several hours. It was then etched in nitric acid and weighed on a microbalance. The current required for a null was measured at 77°K and 4.2°K in a field of 8.35 kg. The values of the corrected current at these temperatures were within 1/2 of 1% of each other, as required, and the value given for 0°K[14] was used for the calibration. The result was

$$\mu(\text{coil}) = 3.93 \times 10^{-3} \text{ emu/milliamp.}$$

To check the calibration, the susceptibility of pure Bi was measured at room temperature. The result was $\chi = -1.348 \times 10^{-6}$ cgs/gram. This falls between two reported values and is considered accurate to about 1/2 of 1%. To insure that the field affecting the sample is only due to the applied field, it is necessary to calculate the field of the pendulum coil. The maximum coil current used is 100 ma. Assuming a solenoidal field and 100 turns/cm, the field due to the current in the pendulum coil is $H = Ni/4\pi \approx 0.8$ Oersted, which is negligible.

The ultimate sensitivity of the magnetometer in the configuration described is 4×10^{-6} emu (about 1 microamp) with a field of 8.35 kOe. It would not be particularly useful to attempt to increase it much further since extreme caution would then be required to eliminate impurities. For example, 0.02 microgram of iron would have a moment of about 4×10^{-6} emu. For very weak specimens, it is better to use a sample

of sufficient size to bring the moment within the measuring range of the instrument. Since the magnetometer described has easily interchangeable pendulum parts, one could construct a quartz tube and coil assembly with a capacity for larger masses. The sample need not be inside the coil, but one must be sure that both the sample and the coil are influenced by the same field gradient.

For measuring the magnetic moments, the foils of the Pd-Co-Si alloys were cut into small rectangular pieces (about 2 mm x 5 mm) so that they could be inserted into the pendulum coil. These pieces were wrapped in an aluminum foil (0.0005" thick) to hold them in position in the pendulum coil while the pendulum was lowered into the specimen chamber. The weights of all the alloy specimens were determined before and after measuring their magnetic moments. The magnetic moments of all the samples were measured between 4.2^{o}K and 300^{o}K, and the magnetic moments of the amorphous samples containing 3, 5, and 7 at.% Co as well as the partly crystallized specimen containing 7 at.% Co were measured at 1.8^{o}K. In addition, the effect of cooling in a 7.5 kOe field was determined at 4.2^{o}K and 1.8^{o}K for the amorphous and partly crystallized samples containing 7 at.% Co. At each temperature and for each applied field, the zero point of the lock-in amplifier (see Appendix A.2) was checked before and after the measurement. If any significant drift occurred, the measurements were repeated.

III. RESULTS

The magnetizations in a field of 8.35 kOe of the amorphous specimens containing 3, 5, 7, 9, 10, and 11 at.% Co are shown in Fig. 7 as a function of temperature and in Fig. 8 as a function of 1/T. The results of the same measurements on the partly crystallized sample containing 7 at.% Co are plotted as a function of temperature and as a function of 1/T in Fig. 9 and Fig. 10, respectively. For the purpose of comparison, the results obtained with the amorphous alloy of the same composition are reproduced in these figures. Representative curves of magnetization (in Bohr magnetons per Co atom) vs applied field at $77^{\circ}K$ and $300^{\circ}K$ are shown in Fig. 11 for alloys containing 7 and 10 at.% Co.

The effect of cooling in a 7.5 kOe field on both the amorphous and partly crystallized samples containing 7 at.% Co was to eliminate almost entirely the low temperature maximum in the magnetization. In the amorphous sample the ratio of the magnetization in a field of 8.35 kOe at $1.8^{\circ}K$ to that at $4.2^{\circ}K$ was changed from 0.81 to 0.94. The effect in the partly crystallized sample was to change the ratio from 0.87 to 0.99.

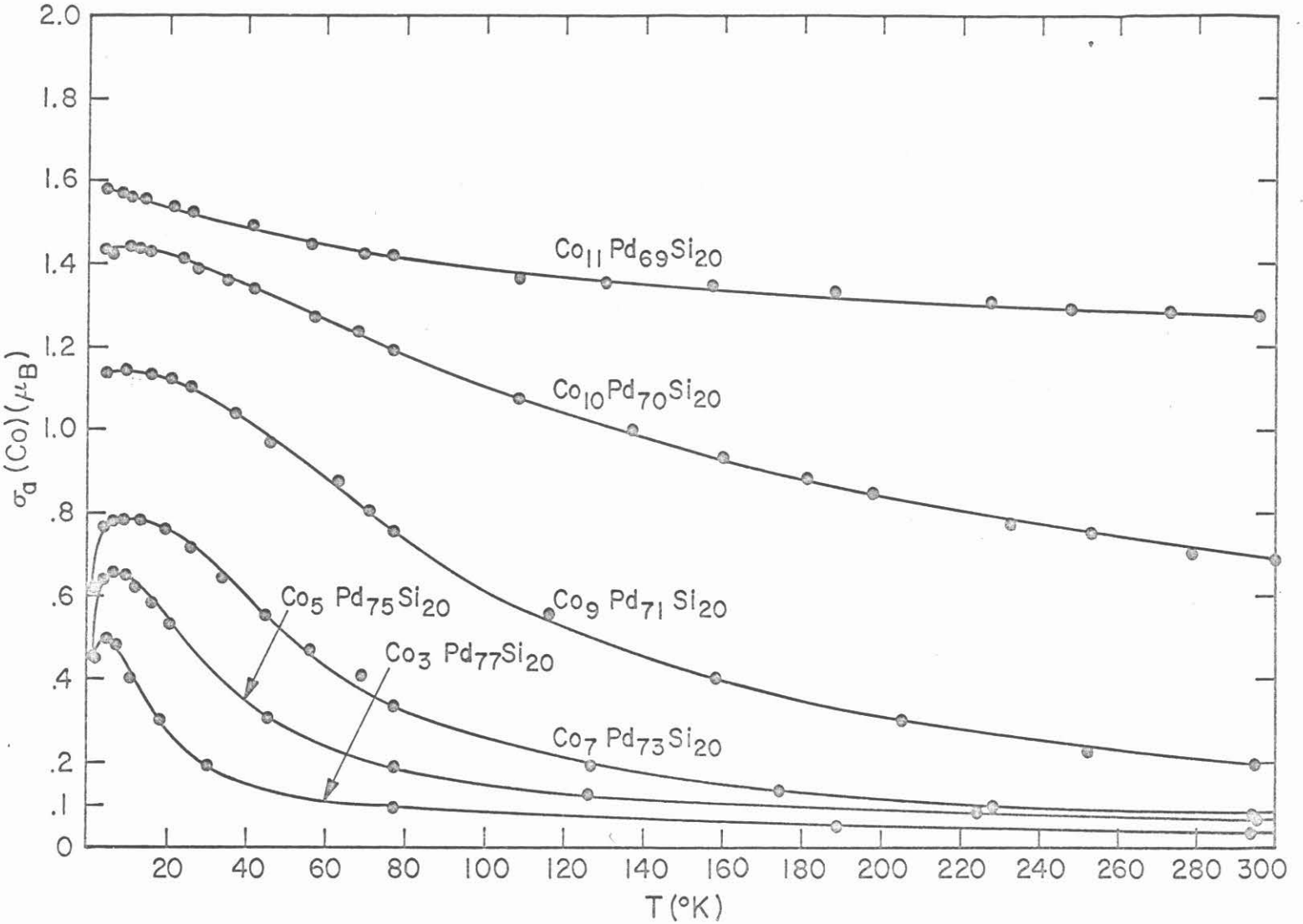

Fig. 7. Magnetization per Co atom of amorphous alloys in a field of 8.35 kOe plotted vs temperature.

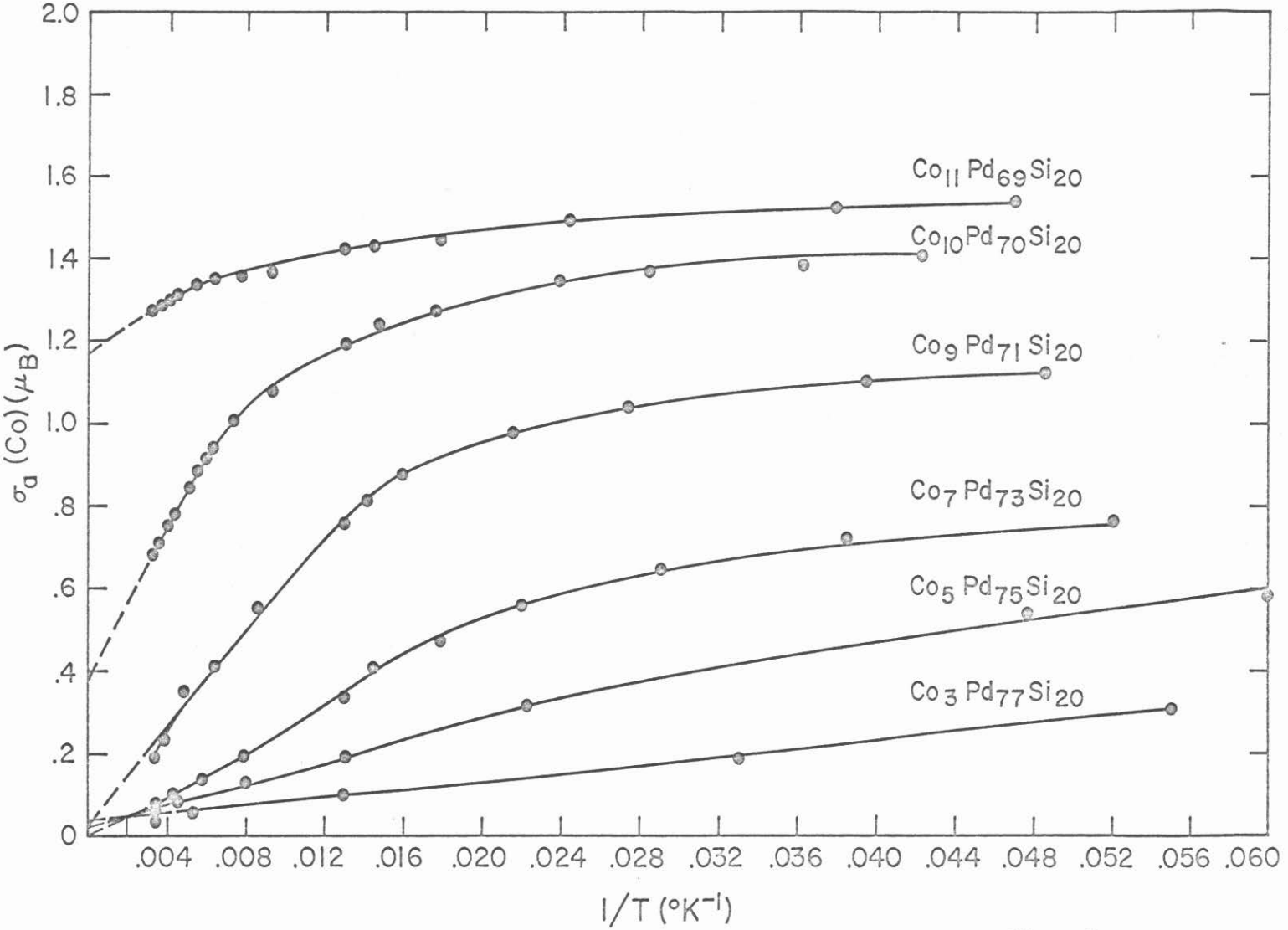

Fig. 8. Magnetization per Co atom of amorphous alloys in a field of 8.35 kOe plotted vs inverse temperature.

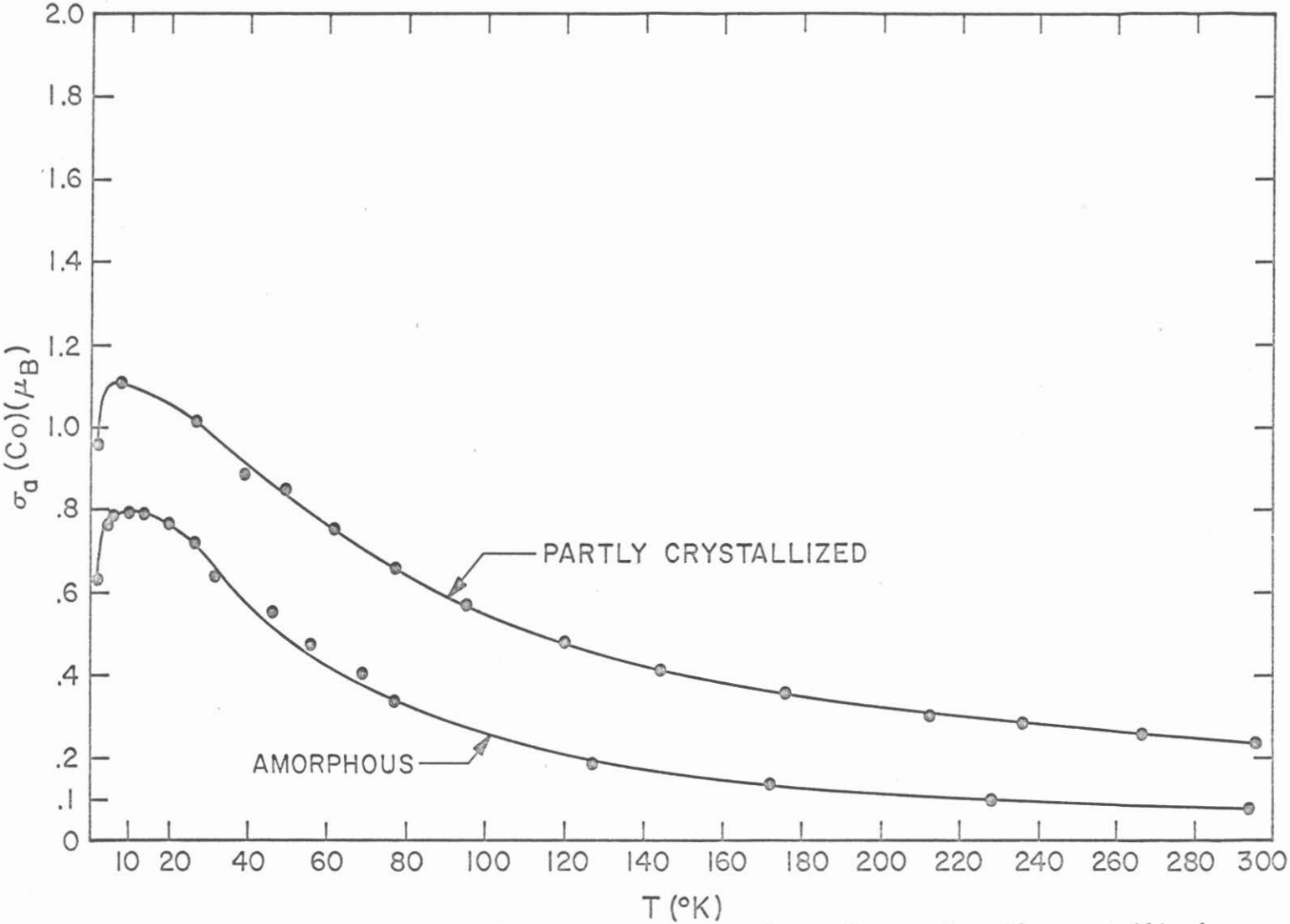

Fig. 9. Magnetization per Co atom of amorphous and partly crystallized alloys containing 7 at.% Co in a field of 8.35 kOe plotted vs temperature.

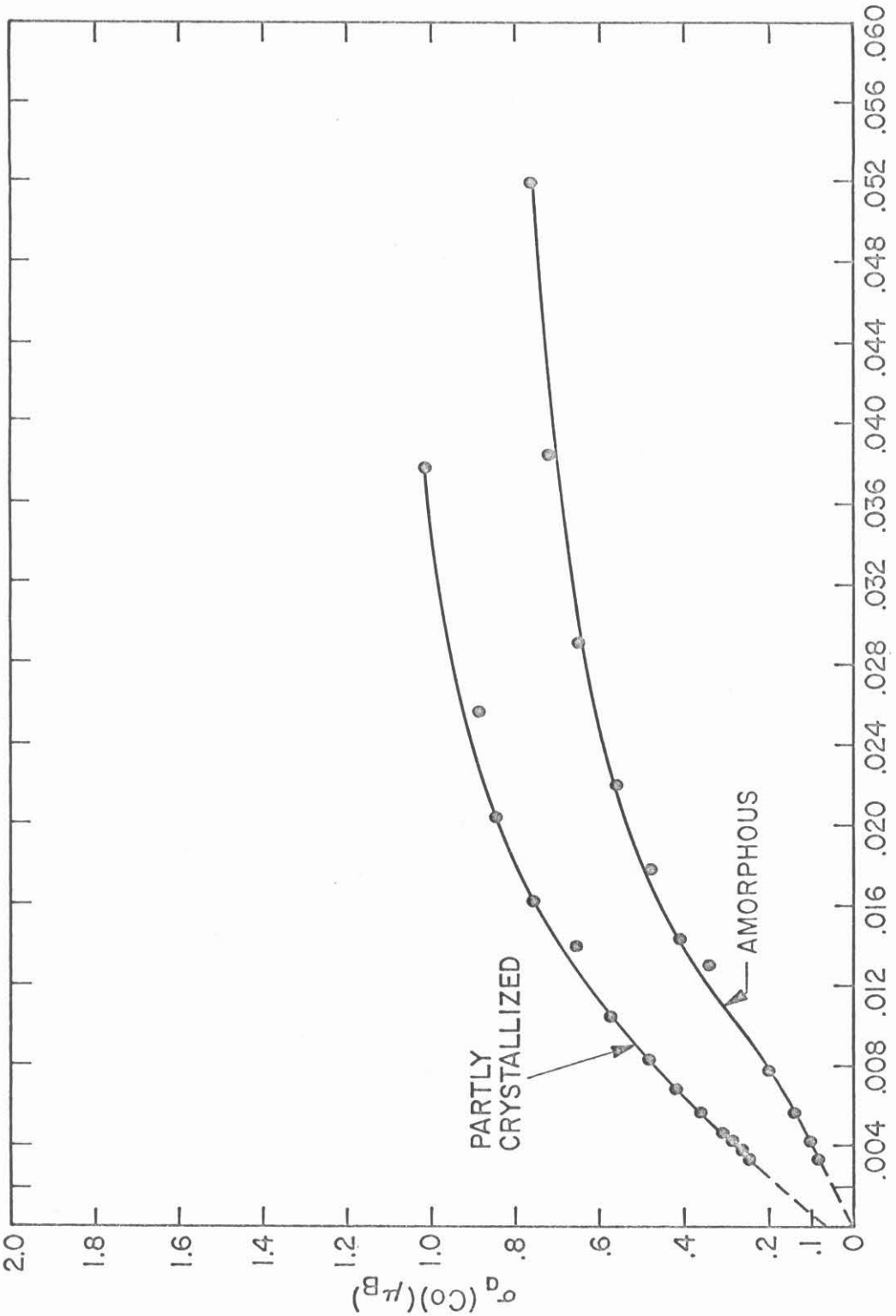

Fig. 10. Magnetization per Co atom of amorphous and partly crystallized alloys containing 7 at.% Co in a field of 8.35 kOe plotted vs inverse temperature.

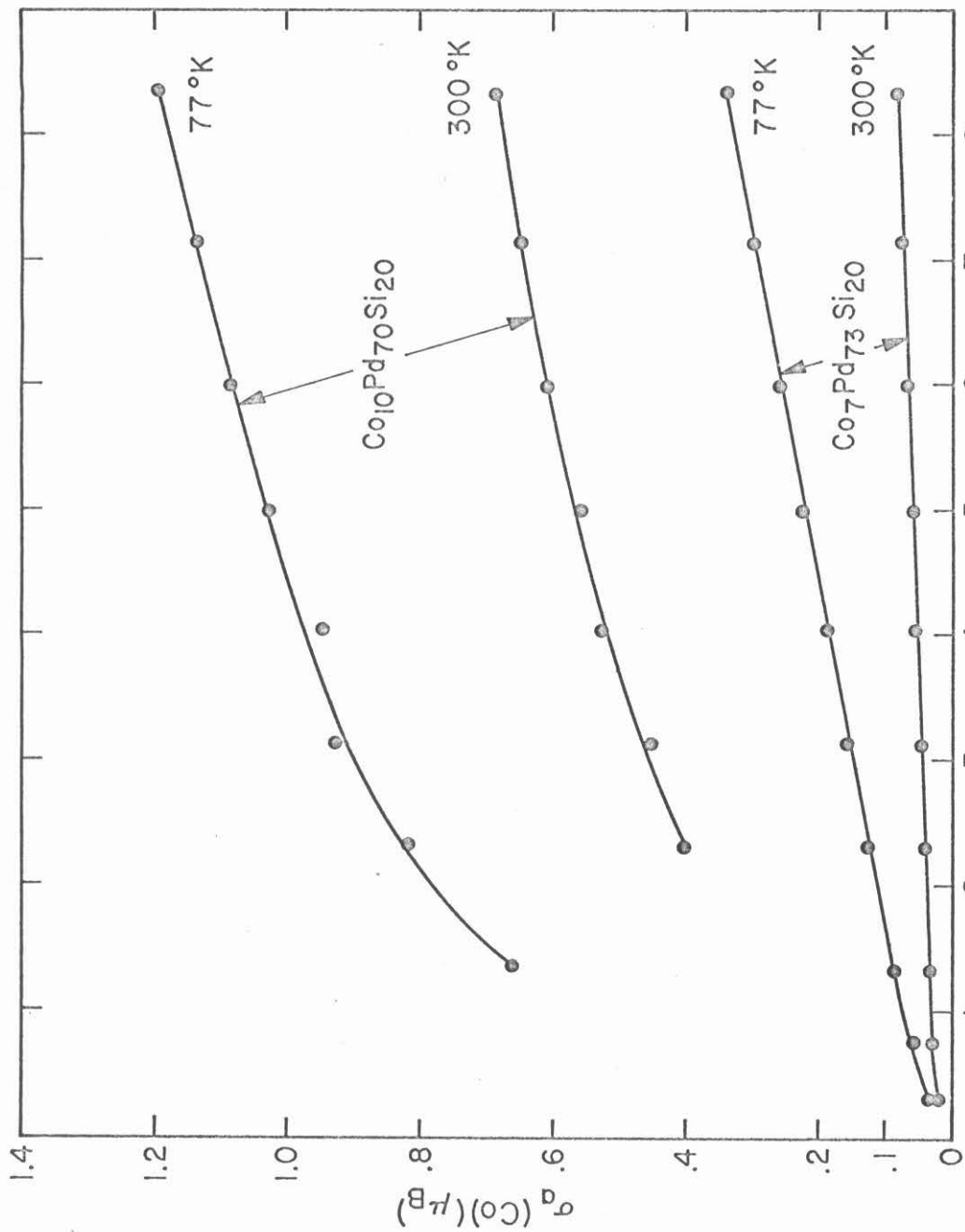

Fig. 11. Representative curves of magnetization per Co atom of amorphous alloys plotted vs applied field.

IV. DISCUSSION

The variation of magnetization with temperature can give information on whether or not a magnetic solid follows Curie's Law, in which case a plot of magnetization vs 1/T should yield a straight line. For the amorphous Pd-Co-Si alloys, this is far from being the case although, as shown in Fig. 8, these curves show a linear portion within certain temperature ranges. For low cobalt content ($Pd_{77}Co_3Si_{20}$) this range is from 4.2 to 300°K. It becomes smaller as the cobalt content is increased and is restricted to near room temperature ($1/T<0.006$) for alloys containing 11 at.% Co. On the basis of Curie's Law, it is possible to calculate a moment per magnetic center. To carry out such a computation, it was assumed, as a first approximation, that the cobalt atoms are sufficiently far apart and there is only one magnetic center per cobalt atom. In this case the susceptibility χ can be expressed by[15]

$$\chi = N p^2 \mu_B^2/3kT + \chi_o$$

in which N is the number of magnetic centers, p is the effective moment per center, and χ_o is the susceptibility of the amorphous Pd-Si alloy without any Co. It is assumed that the moments are due only to electron spins so that $p = g\sqrt{S(S+1)}\mu_B$ and $g = 2$. In the units used, μ_B is taken as unity. Since this alloy is diamagnetic,[16] χ_o can be neglected. Then the local moment is $\mu_a = g S$.

The values of the moment per cobalt atoms, μ_a, calculated in this manner are shown in Fig. 12 as a function of cobalt content. The moments per Co atom for the alloys containing 10 and 11 at.% Co do not fall in line with those calculated for lower Co concentrations. The fact that these two alloys must have a different magnetic structure is also illustrated by the intercept of their magnetization vs 1/T curves shown in Fig. 8. These results would indicate that these two alloys are ferromagnetic at room temperature. On the other hand, the curvature of the magnetization vs temperature plots (see Fig. 7) is clearly opposite to that expected for ferromagnetism. Apparently, part of each sample is paramagnetic and part ferromagnetic, and the relative amounts of each are temperature dependent. Such behavior makes a quantitative analysis of the magnetic moments of these two samples very difficult and a qualitative discussion of their behavior will be attempted at the end of this section.

An important result related to the alloys containing 9 at.% Co or less is the rather large values obtained for the moment per atom of cobalt, μ_a, shown in Fig. 12. The large values of μ_a clearly imply that there must be more than one Co atom per magnetic center. The extrapolations of the magnetization to $1/T = 0$ in Fig. 8 for alloys containing 9 at.% Co or less are so small as to indicate a nearly negligible permanent moment in these alloys. Therefore, the alloys containing 9 at.% Co or less seem to be superparamagnetic over at least part of the temperature range investigated. Superparamagnetism was originally suggested as an explanation for the magnetic behavior observed in certain two phase

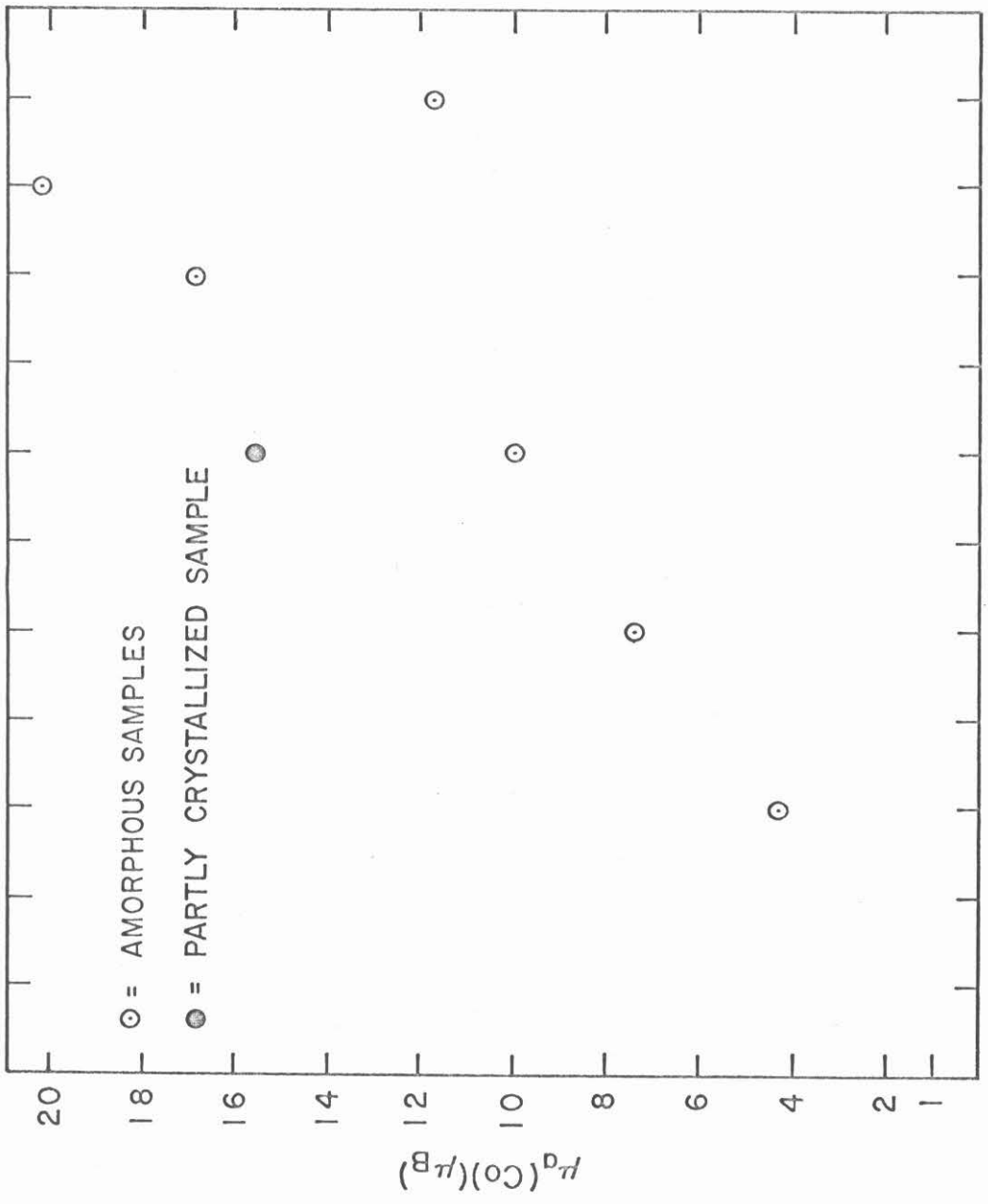

Fig. 12. Moment per atom of Co calculated from the slope of the linear portions of the σ_a vs T^{-1} curves assuming Curie's Law and one magnetic center per Co atom.

alloys consisting of very small ferromagnetic particles in a non-magnetic matrix.[17] The requirements for the ferromagnetic particles are that they be single domains and that thermal fluctuations of the total spin of a particle overcome any tendency toward bulk ferromagnetic phenomena such as remanence and hysteresis. As suggested by Ishikawa,[18] superparamagnetism may also be expected in magnetically dilute single phase alloys where superparamagnetic clusters result from random fluctuations in composition. The clusters are magnetically isolated because they are surrounded by non-magnetic atoms. In such a single phase system, one would not expect a Langevin type dependence of magnetization on H/T since there is a range of cluster sizes. However, the requirement of H/T superposition[17] still holds. In this context, the requirement of H/T superposition means that magnetization curves must be temperature independent to the extent that they superimpose when plotted vs H/T rather than vs H as in the usual magnetization curve. Thus the existence of superparamagnetism may be confirmed by 1) lack of remanence and 2) experimental verification of H/T superposition.

Plots showing H/T superposition have been made for samples containing 9, 7, and 5 at.% Co and are given in Fig. 13. For these plots, a value of σ_{ao} (Co) was obtained by extrapolations to zero applied field of the linear regions of magnetization vs H curves. One would not expect this type of plot to be valid for either high concentrations of Co or low temperatures, where significant curvature occurs in a plot of magnetization vs field at a given temperature (see Fig. 11). One

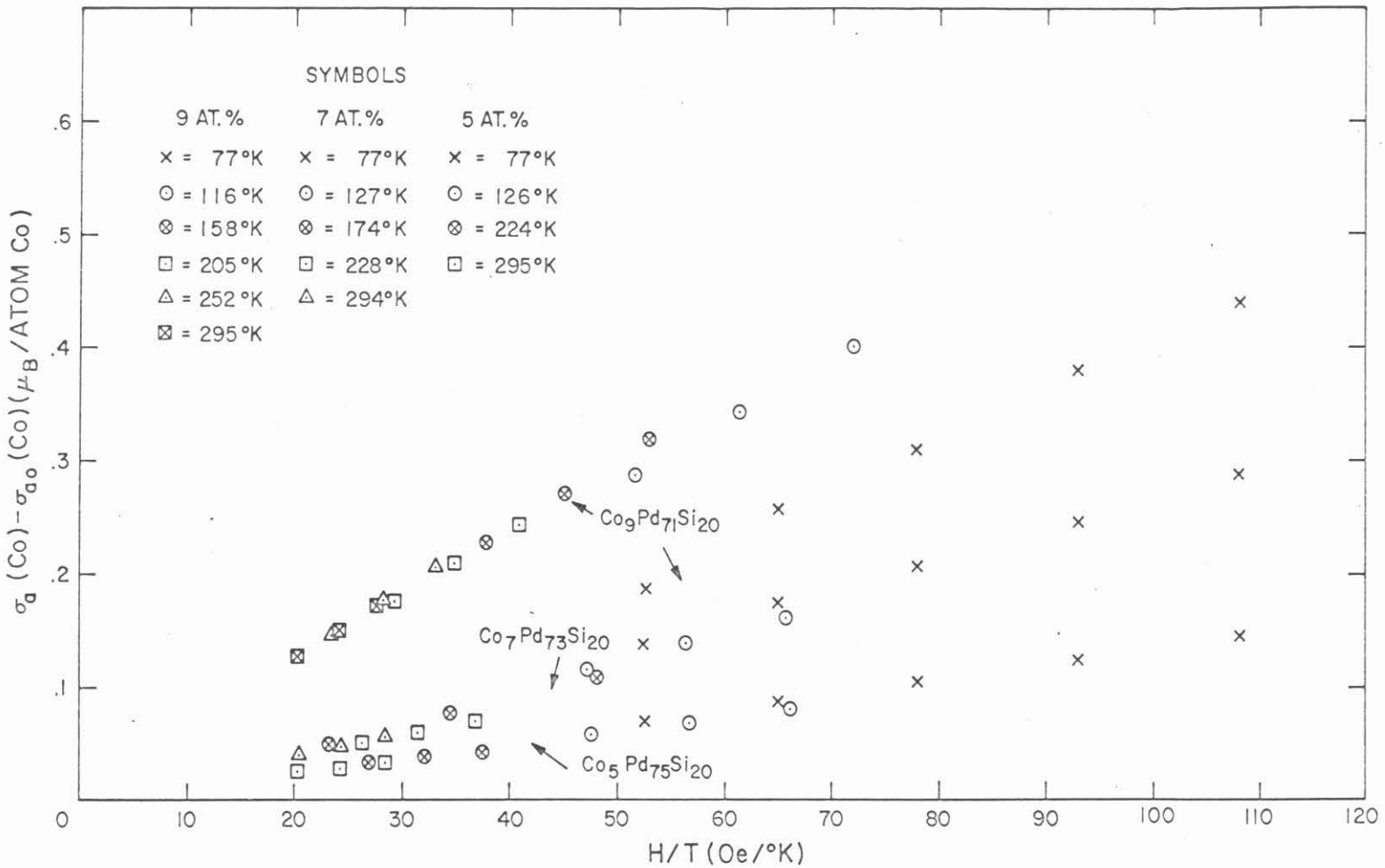

Fig. 13. Plots showing H/T superposition for three of the amorphous alloys.

important source of uncertainty for the H/T plots is the difficulty in assigning a reliable value to the extrapolated value of σ_{ao} (Co). The results shown in Fig. 13, however, seem to indicate that the H/T superposition is reasonably satisfied for alloys containing 9 at.% Co down to about 116°K, and also satisfied for alloys containing 7 and 5 at.% Co down to 77°K. An interpretation of the results obtained at lower temperature is very difficult because the remanence at these temperatures could not be measured accurately enough with the present magnetometer, which does not have a high enough sensitivity for low magnetic fields.

In order to investigate the nature of the superparamagnetic clusters in the amorphous Pd-Co-Si alloys, certain assumptions must be made about atomic moments. First of all, there is considerable evidence that the moment of a Co atom in an alloy tends to be independent of its environment. For example, it was observed by Ehara[19] in NMR measurements that the resonant frequency of Co^{59} in dilute solutions of Co in Pd was virtually the same as in bulk Co, indicating an unchanged Co moment. One would expect Fe to behave similarly to Co in its magnetic properties, and Mössbauer measurements in an Fe-Pd solid solution[20] indicate that the moment at an Fe site is independent of field and temperature. Thus, it appears reasonable to assume that the moment associated with a Co atom in the alloys studied is 1.7 μ_B, as in bulk Co. The high magnetic moments calculated from the experimental data for the amorphous alloys might be due to clusters of Co atoms. There are

several reasons why one would not expect large enough Co clusters to explain the results. In the case of the alloy containing 9 at.% Co, the calculated μ_a is about 17 μ_B. This would require a cluster of $(17/1.7)^2$ or about 100 Co atoms per cluster. Such a number of cobalt atoms in an amorphous matrix could crystallize into a nucleus of crystalline cobalt about 10 A in diameter, and a cobalt crystalline phase would be observed during the early stages of crystallization of an amorphous alloy. Instead, among the first crystalline phases detected after ageing an amorphous alloy containing 7 at.% Co for 96 hours at 325^{o} was a solid solution of Co in Pd (see Fig. 1). The observed diffraction peak corresponding to the (111) reflection was at an angle corresponding to a lattice parameter of about 3.86 A, which is approximately that of a Pd-Co solid solution containing 10 ($\pm$2) at.% Co.[21] If it is assumed that during the early stage of crystallization all the silicon remains in the amorphous matrix, the expected Pd to Co concentration in a Pd-Co solid solution would be 9.6 at.%, which agrees quite well with the X-ray diffraction data.

Thus it appears quite clear that there must be a magnetic moment associated with a Pd atom. A moment can be induced in a Pd atom by the presence of a ferromagnetic atom such as Co.[21] However, the particular Pd atoms which are polarized and the moment to be assigned to such atoms depends strongly on the alloying elements. The possible polarization of Pd atoms in the amorphous alloys will now be discussed. In principle, the intercept at 0 at.% Co of the curve of μ_a vs at.% Co (see Fig. 12) would give the moment associated with an

isolated Co atom plus the moment of any polarized Pd atoms. The curve in Fig. 12 is not accurate enough to obtain a precise value of the intercept, but it is clear that such an intercept could not be much above 1.7 μ_B, which is the moment per Co atom. On this basis, along with the fact that the amorphous alloy without Co ($Pd_{80}Si_{20}$) is diamagnetic, it is assumed that a magnetic moment may exist on a Pd atom only if this atom has two or more Co nearest neighbors. The probability of finding a Pd atom without any Co nearest neighbors can be evaluated if it is accepted that, as shown by Crewdson,[22] the atomic arrangement in an amorphous Pd-Si alloy (based on a study of the radial distribution function) is such that a given Pd atom has, on the average, 11.6 nearest neighbors of any of the two species. If x is the atomic fraction of cobalt in the alloy, the probability for a Pd atom to have zero Co neighbors is $(1-x)^{11.6}$. The probability for one nearest neighbor is $11.6x(1-x)^{10.6}$. Therefore the fraction of Pd atoms with two or more Co nearest neighbors is given by

$$f = 1 - (1-x)^{11.6} - 11.6x(1-x)^{10.6}$$

Since there are $\frac{0.8-x}{x}$ Pd atoms for each Co atom, the effective moment per Co atom is given by

$$\mu_{eff} = \mu_{co} + \mu_{Pd} \cdot \frac{0.8-x}{x} \cdot f.$$

A value of 1.7 μ_B for μ_{Co} is a reasonable assumption, but the value to assign to μ_{Pd} depends on several possible assumptions.

Bozorth, et al.[21] suggest that their magnetic data on dilute

alloys of Co in Pd may be explained by a model in which the 0.6 hole in the 4d band of Pd is completely polarized for all nearest neighbors of a Co atom and nearly unpolarized for more distant atoms. By combining magnetization and neutron diffraction results on PdCo and Pd_3Co, Cable, et al.[23] obtained $\mu_{Pd's}$ of 0.35 μ_B and 0.45 μ_B, respectively, and a μ_{Co} of 2.0 μ_B. Similar work on PdFe and Pd_3Fe yielded $\mu_{Fe's}$ of 2.9 μ_B and 3.0 μ_B, respectively, and a μ_{Pd} of 0.30 μ_B. Their values for Pd_3Fe (ordered) were μ_{Fe}= 3.0 μ_B and μ_{Pd} = 0.45 μ_B. Pickart and Nathans[24] also made neutron diffraction measurements on $FePd_3$ (ordered) and obtained μ_{Fe} = 2.73 μ_B and μ_{Pd} = 0.51 μ_B. Ehara[19] suggests a model for CoPd solid solutions in which a Pd atom with one Co nearest neighbor has a moment of 0.3 μ_B and a Pd atom with two or more nearest neighbors has a moment of 0.6 μ_B (complete polarization). He obtains a fairly good fit to data obtained from saturation magnetization measurements except for very low concentrations of Co. For this situation, he suggests that deviations are due to contributions from more distant Pd atoms. Thus the proper choice of μ_{Pd} to be applied to a calculation of cluster size is not easily made. Experimental data on crystalline solid solutions appear to suggest that Pd atoms are never fully polarized. Furthermore, disordered solutions tend to have a lower μ_{Pd} than ordered phases. For these reasons, a calculation of cluster size for amorphous $Pd_{80-x}Co_xSi_{20}$ has been made under the assumption that μ_{Pd} = 0.30 μ_B and is independent of Co concentration. The values of f and μ_{eff} calculated under these assumptions are plotted in

Fig. 14 as a function of Co concentration. As expected, the extrapolations of the two curves to zero concentration lead to approximately 0 and 1.7 μ_B, respectively.

The average number of Co atoms per cluster is then obtained from the results of the magnetization vs T^{-1} plots (see Fig. 8) and is given by $N(Co)/cluster = (\mu_a/\mu_{eff})^2$, where μ_a = moment per atom of Co obtained from Curie's Law by assuming one magnetic center per atom of Co. Note that the square must be taken quantum mechanically, i.e. $\mu = gS$ implies $\mu^2 = g^2S(S+1)$. By assuming that $g = 2$, a curve representing the average number of Co atoms per cluster is obtained and is shown in fig. 15. It would be logical to expect the curve shown in Fig. 15 to extrapolate to one Co atom per cluster. Although additional data on alloys containing from 1 to 3 at.% Co would be required to substantiate such an extrapolation, such a result is clearly a reasonable possibility.

By heat treating one of the amorphous alloys at a temperature low enough so that long range diffusion does not occur, one may hope to obtain a classical superparamagnetic system in which there are magnetic microcrystals in the amorphous alloy. If one knows the magnetic properties of the microcrystals, one can check the validity of the cluster model. From the X-ray diffraction pattern of an alloy containing 7 at.% Co heat treated at 325°C for 96 hours (see Fig. 1) the dominant crystalline phase can be identified as a Co-Pd solid solution. In a Co-Pd solid solution, one would expect a Pd atom with just

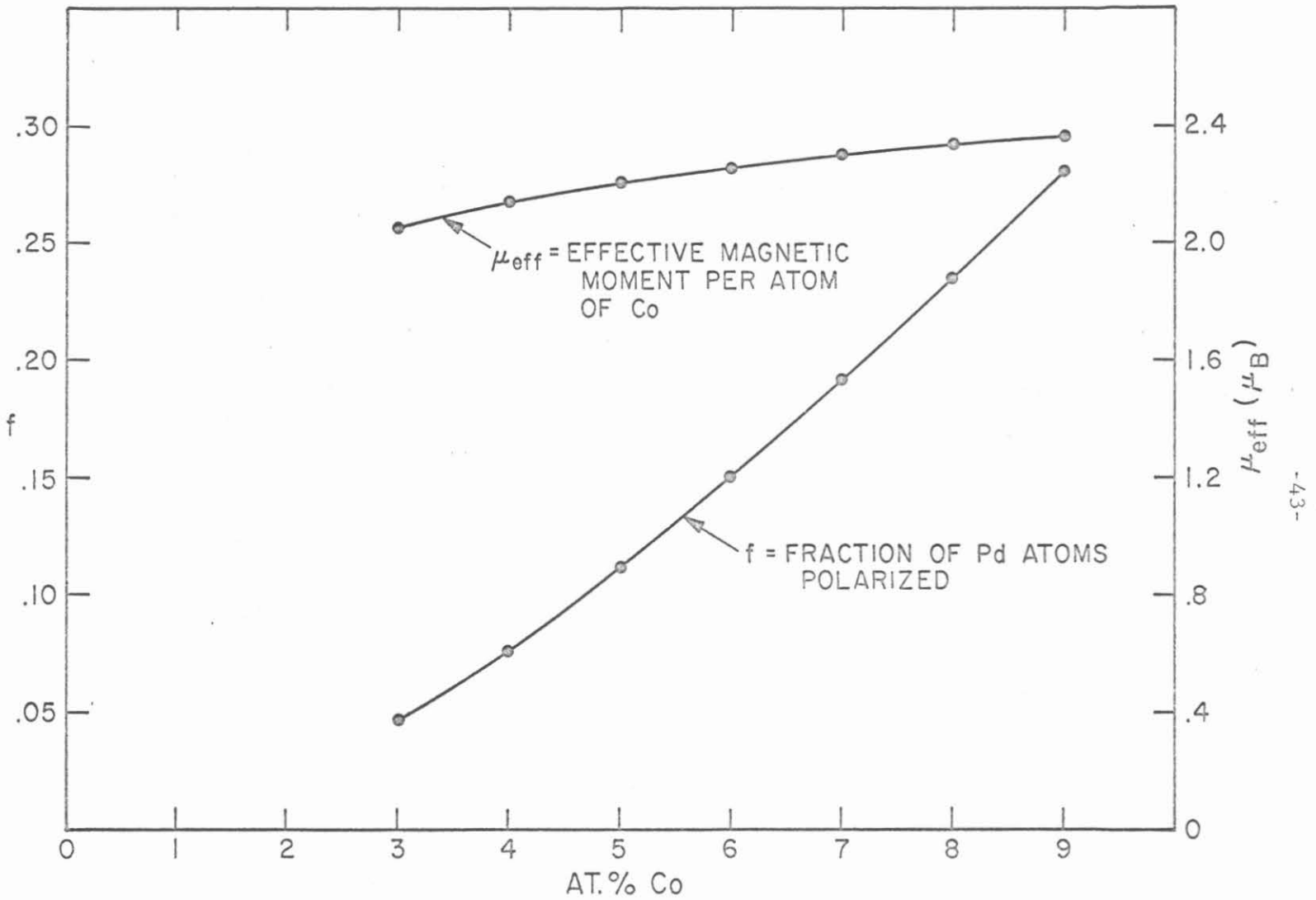

Fig. 14. The fraction of Pd atoms polarized (f) and the effective moment per Co atom (μ_{eff}) plotted vs at.% Co.

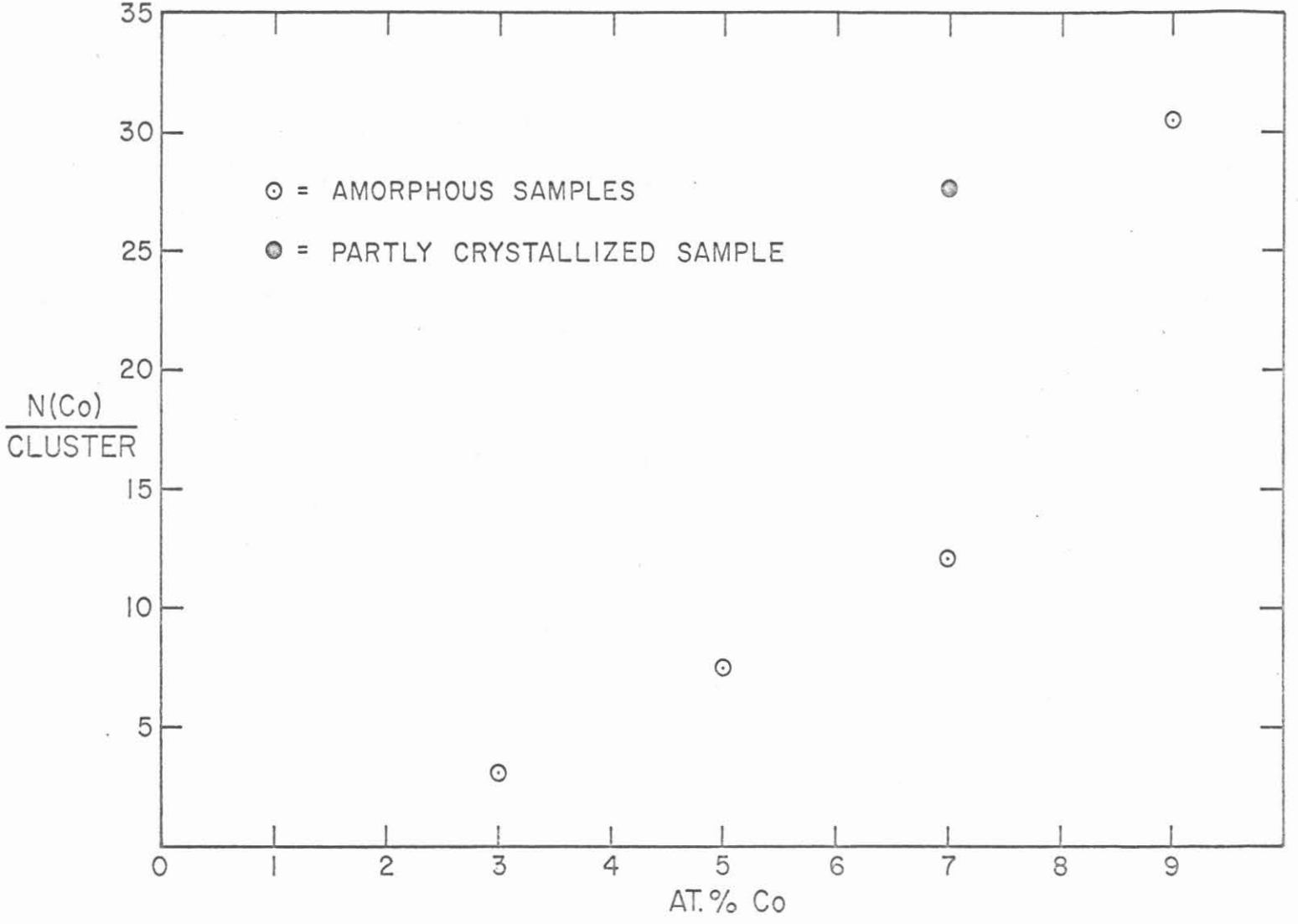

Fig. 15. The number of Co atoms per cluster plotted vs at.% Co.

one or more nearest neighboring Co atoms to be polarized with a moment of about 0.3 μ_B. In addition, the number of nearest neighbors becomes 12 instead of 11.6. Thus, proceeding in the manner used for the amorphous case, $f = 1 - (1-x)^{12}$. If all Si is rejected, $x = 0.096$ yielding $f = 0.602$. Then $\mu_{eff} = 1.7 + 0.3 \times \frac{0.80-0.07}{0.07} \times 0.602 = 3.58$. Therefore, N(Co)/cluster = 13.7. This falls very close to the value calculated for the amorphous sample and is believed to justify the cluster model proposed.

In order to explain the magnetic moments of the amorphous alloys, a model based on superparamagnetism was proposed. However, pure superparamagnetism exists only for those samples containing 9 at.% Co or less and above a certain temperature which depends on the concentration of Co atoms. The deviations from superparamagnetism should be consistent with the cluster model proposed, and this will now be discussed.

At a concentration of about 9 at.% Co, it is noted that the number of Co atoms per cluster rises rapidly. Thus, ferromagnetic behavior should start to occur in this region rather sharply as a function of concentration. This is believed to be responsible for the positive extrapolation of the magnetization to 1/T = 0 (Fig. 8) for alloys containing 10 and 11 at.% Co. These two alloys are ferromagnetic at room temperature. However, ferromagnetic ordering is by no means complete as shown by magnetization vs T curves (see Fig. 7). The curvature for at least part of each curve is opposite to that expected for normal

ferromagnetic behavior. All this is quite consistent with the superparamagnetic model proposed above. Since the cluster size calculated changes rapidly with temperature for higher Co concentrations, one should expect strongly concentration dependent transitions to ferromagnetic behavior. However, a portion of the clusters can still act paramagnetically while the rest of the solid is ordered ferromagnetically. This would explain the curvature observed in the magnetization vs T curves. Further information would be obtained from magnetic measurements above room temperature.

There are two dominant features characteristic of the low temperature behavior of amorphous alloys of $Pd_{80-x}Co_xSi_{20}$. First of all, there is a deviation from linearity in all alloys in the magnetization vs T^{-1} curves (see Fig. 8) (this is not seen in the curve for $Pd_{77}Co_3Si_{20}$ because the abscissa of the graph doesn't extend far enough). The other feature is that alloys containing 7 at.% Co or less show a maximum in magnetization at a fixed field as a function of temperature. The first feature is strongly temperature dependent and the second is not. The maximum is almost completely eliminated by cooling in a magnetic field.

As discussed previously, one cannot assume that ferromagnetic ordering exists at the exact point of deviation from linearity in the magnetization vs T^{-1} curves. However, a significant slope in the magnetization vs field curves (see Fig. 11) persists at the lowest temperatures in all samples at the maximum applied field available in the experiments, and the large deviation from linearity in the magnetization

vs T^{-1} curves cannot be ascribed entirely to non-linear dependence of magnetization on H/T. Thus some interaction between the clusters must occur. If specific heat measurements could be made on the small amount of material available from amorphous foils, considerable additional information could be gained.[25] It is, however, clear that the onset of cluster interaction is quite temperature dependent, expecially near a concentration of 9 at.% Co. This is in qualitative agreement with the results obtained above for cluster size (see Fig. 15), which varies rapidly in this range of concentration.

The maximum in magnetization observed at low temperatures may be ascribed either to a form of antiferromagnetic coupling between a portion of the moments present or to a form of magnetocrystalline anisotropy applicable to an amorphous alloy. The elimination of a maximum due to anisotropy by the use of cooling in a magnetic field is analogous to the magnetic cooling of some types of permanent magnets. That cooling in a magnetic field can eliminate a maximum due to antiferromagnetic coupling has been shown by Nesbitt, et al.[26] for the compound Mn_2Tb. It is not possible with the equipment available to distinguish between these two possible effects. However, the effect of cooling in a magnetic field clearly eliminates the possibility of a drop in magnetization due to a change in atomic moments. Antiferromagnetic ordering has been suggested as an explanation for the maximum in magnetization observed in dilute alloys of Mn in Cu[27] and Fe in Au,[28] but cooling in a magnetic field has no effect in these alloys.

Another type of transition to antiferromagnetism occurs in alloys displaying exchange inversion such as Fe-Rh alloys.[29] In these alloys, there is a transition from a ferromagnetic state to an antiferromagnetic state as the temperature is lowered. This is in contrast to Mn-Cu and Fe-Au dilute alloys, which do not display true bulk ferromagnetism at any temperature. However, in the case of Fe-Rh alloys, the temperature of exchange inversion is very concentration dependent, in contrast to amorphous $Pd_{80-x}Co_xSi_{20}$ alloys. Very high pulsed fields can eliminate the antiferromagnetic state in Fe-Rh alloys, but the effect of cooling in a magnetic field is not known. High field, hysteresis loop, thermal hysteresis, heat capacity, and low temperature (below $4.2^{\circ}K$) resistivity measurements could be useful in determining the origin of the maximum in magnetization. It might also be useful to prepare dilute alloys of the type $Pd_{80-x}Fe_xSi_{20}$.[3] If magnetic measurements on these alloys show a maximum similar to $Pd_{80-x}Co_xSi_{20}$, Mössbauer Effect measurements might be useful in elucidating its origin.

V. CONCLUSIONS

The magnetic moments of ternary amorphous Pd-Co-Si alloys have been studied. The amount of Si was kept fixed at 20 at.% and Co was substituted for Pd in amounts from 3 at.% to 11 at.%. The results of the study showed that the magnetic moments depended strongly on both composition and temperature. Since Curie's Law was followed over part of the temperature range for all of the samples and since the local moments calculated from Curie's Law were much too high to be due to atomic moments of individual Co atoms, a model based on superparamagnetism in a homogeneous system is proposed. Both Co and Pd are known to be magnetically active in alloys but some assumptions about their magnetic moments are necessary. From the experimental data it appears reasonable to assume that in the present alloys all the Co atoms have a fixed moment of 1.7 μ_B (as in bulk Co) and that the Pd atoms which have two or more Co nearest neighbors have a magnetic moment of 0.3 μ_B. From this statistical model an average size for a superparamagnetic cluster was calculated. From this calculation, it was deduced that the cluster size increases very rapidly when the Co concentration reaches about 9 at.%. This is precisely the concentration beyond which ferromagnetism (as determined by a positive intercept at $1/T = 0$ in the magnetization vs 1/T plots) exists at room temperature. Further experimental evidence for the validity of the cluster model was provided by experiments on a partly crystallized alloy. The main crystalline

phase was identified as a Pd-Co solid solution and, by using atomic moments valid for this phase, a cluster size was determined. Although the measured magnetic moments of the partly crystalline alloy were much higher than those of the corresponding amorphous alloy, the calculated cluster sizes were very close. The deviations from superparamagnetic behavior observed at lower temperatures and higher concentrations of Co may be ascribed to interactions between clusters. The type of interaction leading to a maximum in magnetization at low temperatures in alloys containing 7 at.% or less cannot be determined precisely by the experiments performed. Calorimetric and resistivity measurements might be of value for this purpose. The clusters themselves might be investigated directly by the use of very high magnetic fields or by performing nuclear magnetic resonance measurements on alloys containing Pd^{105}. The effect of the Si concentration on the magnetic properties is unknown and more information in this area might be obtained by varying the Si content. Unfortunately, the range of silicon concentrations within which these alloys can be quenched into an amorphous phase is rather narrow (from 15.5 to about 23 at.%). Thus, the experiments performed raise a number of significant questions. However, a fairly crude model seems to have yielded quite consistent results in the amorphous ternary alloys with two magnetically active species.

REFERENCES

1. A. I. Gubanov, Soviet Physics, Solid State, 2, 468 (1960).

2. S. Mader and A. S. Nowick, Applied Physics Letters, 7, 57 (1965).

3. C. C. Tsuei and Pol Duwez, J. Appl. Phys., 38, 4096 (1967).

4. Pol Duwez, R. H. Willens, and R. C. Crewdson, J. Appl. Phys.,36, 2267 (1965).

5. Pol Duwez, Transactions of the ASM, 60, 607 (1967).

6. W. Sucksmith, Phil. Mag., 8, 158 (1929).

7. W. Sucksmith, Proc. Roy. Soc., 170, 551 (1939).

8. N. Lundquist and H. P. Myers, J. Sci. Instrum., 39, 154 (1962).

9. D. E. Soule, C. W. Nezbeda, and A. W. Czanderna, Rev. Sci. Instr., 35, 1504 (1964).

10. R. M. Bozorth, H. J. Williams, and Dorothy E. Walsh, Phys. Rev., 103, 572 (1956).

11. P. Jongenburger and C. W. Berghout, Appl. Sci. Res. Section B, Vol. 7, 366 (1961).

12. R. C. Sherwood, private communication.

13. J. C. Sanchez and W. V. Wright, Instr. Soc. of America, Conference Preprint, 37-SL61 (1961).

14. R. M. Bozorth, Ferromagnetism, D. Van Nostrand Company, Inc. (1951), p. 867.

15. P. A. Wolff, P. W. Anderson, A. M. Clogston, B. T. Matthias, M. Peter, and H. J. Williams, J. Appl. Phys., 33, 1173 (1962).

16. R. H. Willens, private communication.

17. C. P. Bean and J. D. Livingston, J. Appl. Phys., 30, 120S (1959).

18. Y. Ishikawa, J. Appl. Phys., 35 (part 2), 1054 (1964).

19. Shaw Ehara, J. Phys. Soc. Japan, 19, 1313 (1964).

20. P. P. Craig, R. C. Perisho, R. Segnan, and W. A. Steyert, Phys. Rev.,138, A1460 (1965).

21. R. M. Bozorth, P. A. Wolff, D. D. Davis, V. B. Compton, and J. H. Wernick, Phys. Rev., 122, 1157 (1961).

22. R. C. Crewdson, Ph.D. Thesis, California Institute of Technology, (1966).

23. J. W. Cable, E. O. Wollan, W. C. Koehler, and M. K. Wilkinson, J. Appl. Phys., 33, 1340 (1962).

24. S. J. Pickart and R. Nathans, J. Appl. Phys., 33, 1336 (1962).

25. H. Sato, A. Arrott, and R. Kikuchi, J. Phys. Chem. Solids, 10, 19 (1959).

26. E. A. Nesbitt, H. J. Williams, J. H. Wernick and R. C. Sherwood, J. Appl. Phys., 34, 1347 (1963).

27. A. W. Overhauser, J. Phys. Chem. Solids, 13, 71 (1960).

28. R. Tournier and Y. Ishikawa, Physics Letters, 11, 280 (1964).

29. J. Kouvel and C. Hartelius, J. Appl. Phys., 33, 1343 (1962).

APPENDIX

A.1. Analysis of the Strain Gage - Pendulum System

The moving section of the pendulum consists of a bending beam which is fixed at the top and a rigid member which is attached to the bottom of the bending beam. Silicon strain gages are bonded on both sides of the bending beam and wired such that their outputs are additive. For the purpose of this analysis, the rigid member is replaced by a point mass positioned at its center of mass. The magnetic force is also assumed to be a point force applied at the bottom of the rigid member. A diagram of the bending beam is shown in Fig. A.1.

Let x = coordinate of point along the phosphor bronze spring and y = coordinate of deflection. The origin is at the bottom of the spring. The parameters involved are:

E = modulus of elasticity

I = area moment of inertia

M = total mass of pendulum assumbly

F = force on coil (due to field)

L = coordinate of center of coil

L'= coordinate of top of beam

R = coordinate of center of mass

g = acceleration due to gravity

Then by balancing torques,[1]

$$EI\frac{d^2y}{dx^2} + Mg(R+x)\frac{dy}{dx} = -F(L+x)$$

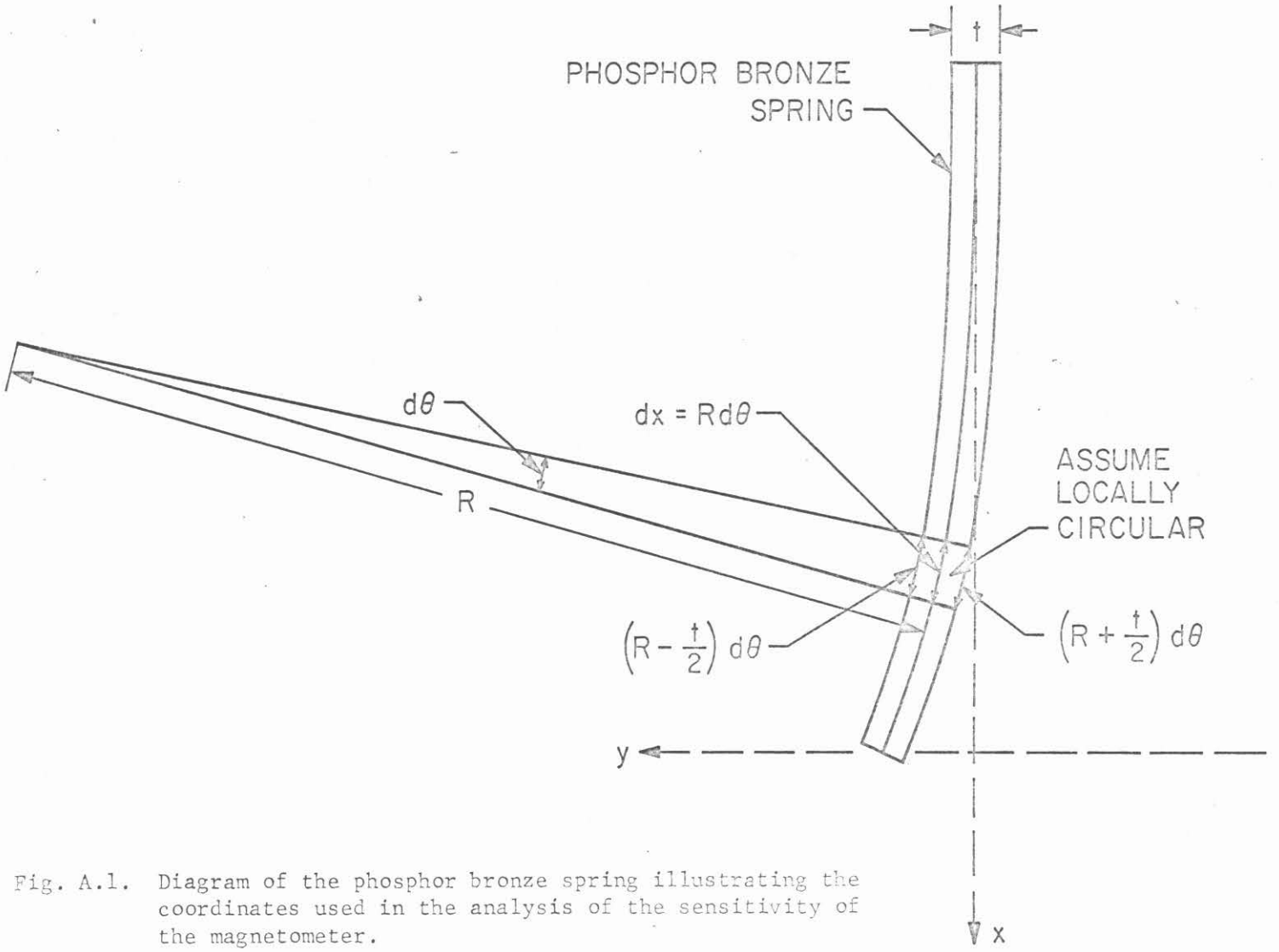

Fig. A.1. Diagram of the phosphor bronze spring illustrating the coordinates used in the analysis of the sensitivity of the magnetometer.

where $-L' < x < 0$. This is a first order linear differential equation in $\frac{dy}{dx}$ whose solution is:[2]

$$\frac{dy}{dx} = -\left\{\exp\left[-\int \frac{Mq}{EI}(R+x)dx\right]\right\}$$

$$\times \int_c^x \frac{F}{EI}(L+x)\left\{\exp\left[\int \frac{Mq}{EI}(R+x)dx\right]\right\}dx$$

where C is an arbitrary constant to be determined by the boundary condition:

$$\left.\frac{dy}{dx}\right|_{x=-L'} = 0.$$

$$\frac{dy}{dx} = -\frac{F}{EI}\exp\left[-\frac{Mq}{EI}\left(Rx + \frac{x^2}{2}\right)\right]$$

$$\times \int_c^x (L+x)\exp\left[\frac{Mq}{EI}\left(Rx + \frac{x^2}{2}\right)\right]dx.$$

$$\int_c^x (\cdots)dx = \exp\left[-\frac{MqR^2}{2EI}\right]$$

$$\times \left[\frac{EI}{Mq}\exp\left[\frac{Mq}{2EI}(R+x)^2\right]\right.$$

$$\left. + (L-R)\sqrt{\frac{2EI}{Mq}}\int_0^{\sqrt{\frac{Mq}{2EI}}(R+x)} e^{u^2}du + C'\right].$$

From the boundary condition,

$$C' = -\frac{EI}{Mg} \exp\left[\frac{Mg}{2EI}(R-L')^2\right] - (L-R)\sqrt{\frac{2EI}{Mg}} \int_0^{\sqrt{\frac{Mg}{2EI}}(R-L')} e^{u^2} du .$$

$$\frac{dy}{dx} = -\frac{F}{Mg}\left[1 - \exp\left[\frac{Mg}{2EI}\left\{(R-L')^2 - (R+x)^2\right\}\right] + \left\{\exp\left[\frac{Mg}{2EI}(R+x)^2\right]\right\}(L-R)\sqrt{\frac{2Mg}{EI}} \times \left\{\int_0^{\sqrt{\frac{Mg}{2EI}}(R+x)} e^{u^2} du - \int_0^{\sqrt{\frac{Mg}{2EI}}(R-L')} e^{u^2} du \right\}\right].$$

From Fig. (6) it may be seen that the net change in length on either side = t/2 $d\theta$ where t = thickness of the bending beam. Therefore the strain is given by

$$\epsilon = \frac{\frac{t}{2} d\theta}{dx} = \frac{t}{2} d\left(\frac{dy}{dx}\right) = \frac{t}{2} \frac{d^2y}{dx^2} .$$

The above value is the strain at a point. In reality, strain gages have a finite active length which is difficult to obtain exactly. The active length in the gages used appears to be less than 1/8 inch so the use of a point strain in these calculations seems justified.

From the original differential equation:

$$\frac{d^2y}{dx^2} = -\frac{F}{EI}(L+x) - \frac{Mq}{EI}(R+x)\frac{dy}{dx} .$$

$$\frac{\epsilon}{F} = -\frac{t}{2EI}(L+x) + \frac{t}{2EI}(R+x)$$

$$\times\left[1 - \exp\left[\frac{Mq}{2EI}\left\{(R-L')^2 - (R+x)^2\right\}\right]\right]$$

$$+\left\{\exp\left[\frac{Mq}{2EI}(R+x)^2\right]\right\}(L-R)\sqrt{\frac{2Mq}{EI}}$$

$$\times\left\{\int_0^{\sqrt{\frac{Mq}{2EI}}(R+x)} e^{u^2}du - \int_0^{\sqrt{\frac{Mq}{2EI}}(R-L')} e^{u^2}du\right\}\Bigg].$$

Assume that the strain gages measure the strain at $x = \frac{-L'}{2}$.

$$\frac{\epsilon\left(-\frac{L'}{2}\right)}{F} = -\frac{t}{2EI}\left(L-\frac{L'}{2}\right) + \frac{t}{2EI}\left(R-\frac{L'}{2}\right)$$

$$\times\left[1 - \exp\left[\frac{Mq}{2EI}\left(\frac{3}{4}L'^2 - RL'\right)\right]\right]$$

$$+\left\{\exp\left[\frac{Mq}{2EI}\left(R-\frac{L'}{2}\right)^2\right]\right\}(L-R)\sqrt{\frac{2Mq}{EI}}$$

$$\times\left\{\int_0^{\sqrt{\frac{Mq}{2EI}}\left(R-\frac{L'}{2}\right)} e^{u^2}du - \int_0^{\sqrt{\frac{Mq}{2EI}}(R-L')} e^{u^2}du\right\}\Bigg],$$

or $$\frac{\epsilon\left(-\frac{L'}{2}\right)}{F} = (a) + (b)\left[1 - (c) + (d)\left\{(e) - (f)\right\}\right].$$

Numerical calculation of sensitivity:

$I = 1/12\ wt^3$

w = width of phosphor bronze spring = 0.318 cm

t = thickness = 0.0127 cm

$M = 85.4$ g

$E = 11 \times 10^{11}$ dynes/cm^2

$g = 980$ cm/sec^2

$L = 100.2$ cm

$L' = 2.54$ cm

$R = 2.6$ cm - This was obtained by finding the mass and balance point of the quartz rod plus coil and the counter-weight tube plus locking ring and combining them in a weighted average.

H = magnetic field = 8 kOe

$\frac{dH}{dy}$ = magnetic field gradient = 300 Oe/cm at H = 8 kOe.

Both H and $\frac{dH}{dy}$ were measured directly with a Hall Effect probe.

G.F. = gage factor for the silicon strain gages = $\frac{\Delta R/R}{\epsilon}$ where

R = resistance. G.F. $\approx$ 100 from data supplied by the manufacturer.

m = magnetic moment

V_{out} = output voltage from strain gage bridge circuit.

$V_{s.g.}$ = voltage across each strain gage = 0.5 volt.

Thus, (a) $= 1.05 \times 10^{-5}$

(b) $= 1.412 \times 10^{-7}$

(c) = 3.42

(d) = 47.45

$$(e) = \int_0^{1.113} e^{u^2}\, du = 1.809$$

$$(f) = \int_0^{0.0502} e^{u^2}\, du = 0.050$$

$$\frac{\epsilon(\frac{-L'}{2})}{F} = -1.05 \times 10^{-5} + 1.15 \times 10^{-5} = 1.0 \times 10^{-6} \text{ dyne}^{-1}$$

Since both gages are active:

$$V_{out} = 2V_{s.g.} \frac{\Delta R}{R} = 2V \cdot (G.F.) \cdot \epsilon$$

$$\frac{V_{out}}{F} = 1.0 \times 10^{-4} \text{ volt/dyne}$$

$$F = \left|\nabla (\text{Energy})\right| = \left| \nabla (m \cdot H)\right| = m \frac{dH}{dy}$$

$$\frac{V_{out}}{m} = 3.0 \times 10^{-2} \text{ volt/emu} = 30 \text{ mV/emu}$$

The sensitivity was measured directly at H $\approx$ 8 kOe by changing the current in the magnetometer coil by a known amount and observing the change in output voltage. This measurement yielded:

$$\frac{\Delta V_{out}}{\Delta m} \approx \frac{10 \text{ mV}}{\text{emu}}$$

Possible reasons for the discrepancy between measured and calculated values are:

a) The glue used to attach the strain gages to the phosphor bronze spring may significantly affect both E and t.

b) The calculation involves a difference of two close numbers so that it is very sensitive to certain parameters which may not be known with sufficient accuracy.

c) Both the assumption of point strain and the point at which the strain was calculated may be in error.

Various limiting cases:

a) Mg = 0

$$\frac{\epsilon}{F} = \frac{-t}{2EI}\left(L - \frac{L'}{2}\right) = -1.05 \times 10^{-5} \text{ dyne}^{-1}$$

This yields an increase of a factor of 10 over the above calculated value. Thus, judicious attempts to reduce the mass (without changing other parameters) would be useful.

b) R = L, i.e. - all mass concentrated at the bottom of the pendulum.

$$\frac{\epsilon}{F} \approx \frac{-tL'}{2EI} = -2.77 \times 10^{-7} \text{ dyne}^{-1}$$

Thus, the calculated sensitivity was increased by a factor of 4 in moving the center of mass upward to R = 2.6 cm.

c) Let L→2L

$$\frac{\epsilon}{F} = -2.3 \times 10^{-6}$$

Thus, doubling the pendulum length increases the sensitivity by a little more than a factor of 2. Since it would be difficult to do so without increasing Mg, there is probably little point in

using a longer pendulum.

d) Let R = -x. This yields the same result as having zero mass. This is easy to do and could become very worthwhile if a magnetometer coil with a very small moment were built. The increase in sensitivity will be offset somewhat by a lessening in the damping effect of the phosphor bronze spring and some experimentation to determine an optimum R would be necessary.

e) Let R go above -x. The sensitivity will increase in an exponential manner. An absolute upper limit to R is determined by the condition that a stable equilibrium exist when F = 0.

Calculation of critical stability:

Let F = restoring force in bending beam at x = 0.

Mg $(R\theta+y)$ = FL' by torque balance about top of bending beam.

$$\theta \approx \frac{dy}{dx}\Big|_{x=o} = \frac{1}{2}\ \frac{FL'^2}{EI}$$

$$y(x=o) = -\frac{1}{3}\frac{FL'^3}{EI} - \frac{1}{3}\frac{FL'^3}{EI}$$

$$Mg\left[R\cdot 1/2\ \frac{FL'^2}{EI} - \frac{1}{3}\frac{FL'^3}{EI}\right] = FL'$$

$$R = \frac{2}{3}L' + \frac{2EL}{MgL'}$$

For the above numbers,

$$R = \frac{2}{3} \times 2.54 + \frac{2}{1.40 \times 2.54}\ \text{cm}$$

$$= 1.69 + 0.56 = 2.25\ \text{cm}$$

Therefore, the maximum allowable value for R is 2.25 cm above the

bottom of the phosphor bronze spring.

A.2. Measurement of Strain Gage Output

An a.c. bridge circuit utilizing a lock-in amplifier as a detector was judged to be the best way to measure the strain. By using the strain gages as two adjacent arms of the bridge, the effect of temperature variations on bridge balance is lessened if the characteristics of the strain gages are similar.

In choosing the bridge components, the major problems considered were temperature and frequency stability. In the former, it is of course desirable that the temperature coefficient of impedance be small. In the latter, it is desirable that the bridge balance be independent of frequency. The final design chosen is shown in Fig. A.2.

The detector is a Princeton Applied Research model HR-8 lock-in amplifier. It is an almost ideal instrument for this type of measurement. Since detection is phase sensitive and since the output is fed into a variable time constant filter, both the effect of noise and random swinging of the pendulum are greatly diminished. The sensitivity of the instrument is actually well beyond the level required, enabling operation at a low oscillator output. Two preamplifiers are available - type A for high and type B for low input impedance. The latter was employed for this bridge. Since the signal is fed through a tuned amplifier prior to cross-correlation with the oscillator output, analysis of noise as a function of frequency is very simple. The frequency chosen for operation was 1 kc. The noise level at this frequency was

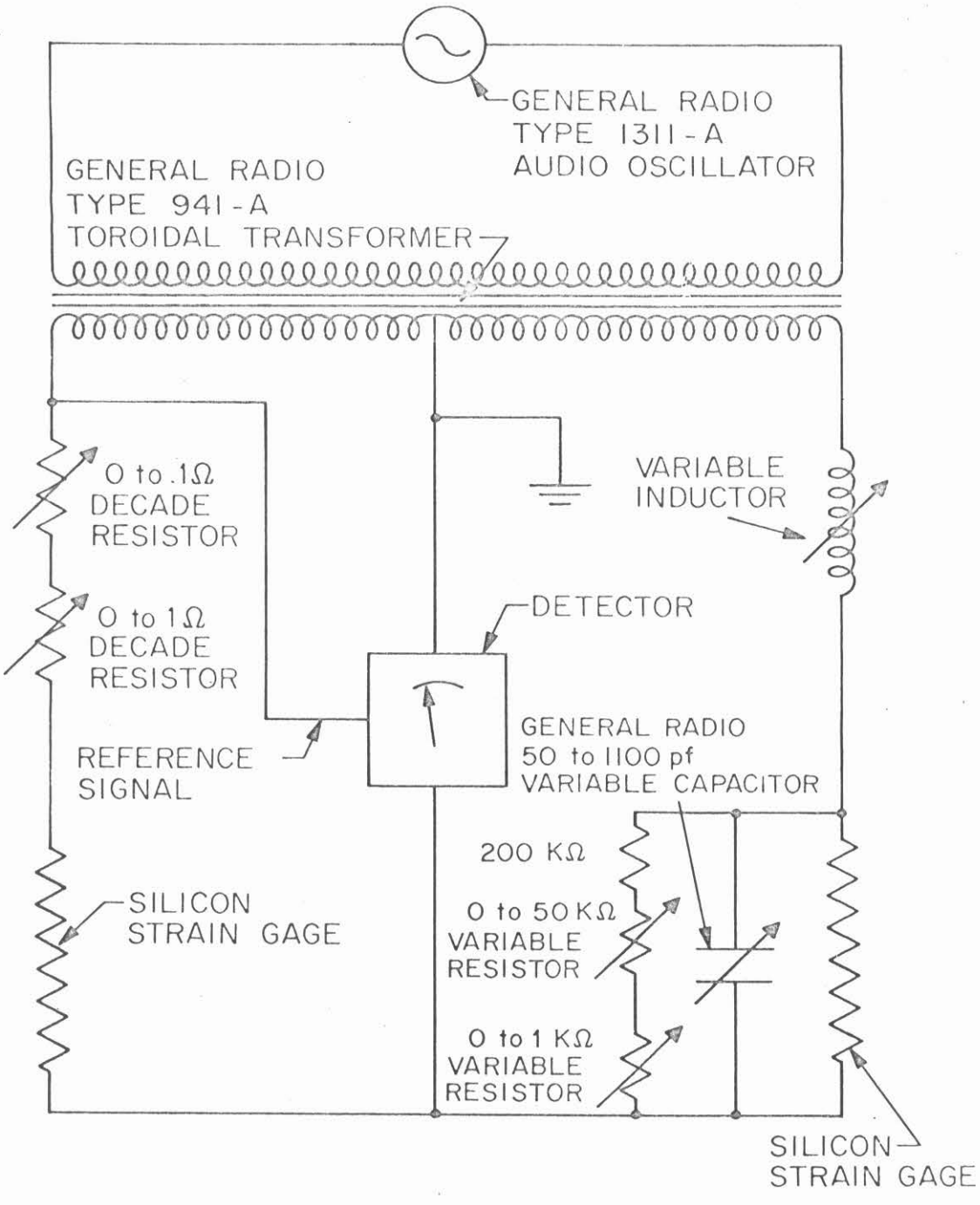

Fig. A.2. Diagram of the electrical circuit used to measure the strain in the phosphor bronze spring.

low and the input impedance not far above that recommended for the type B preamplifier.

This type of circuit is very convenient since the transformer itself serves as the required two legs of the bridge. In addition, the effect of lead wire capacitance on frequency stability is quite small in this type of bridge. By placing ground at the center of the secondary on the transformer, lead wire capacitances either have the effect of being in parallel with one winding on the transformer or in parallel with the detector. In the latter case, the impedance due to the capacitance is certainly high enough not to act as a load on the lock-in amplifier. In the former case, the transformer winding appears as a short circuit to the capacitance so that it again has little effect.

Since the reactances of the two secondary windings on the transformer are not perfectly matched, an external element is necessary to achieve reactive balance. If the element is inductive, reactive balance will be independent of frequency. The amount of inductance necessary was determined approximately by placing a variable inductor in series with the transformer. The amount necessary was about 450 μh. An inductor was then wound on a length of 3 cm pyrex tubing. Two 200 μh windings were made and wired together in an opposing sense to minimize noise pick-up. Then 40 μh, 30 μh, 20 μh, and 10 μh windings were made. This yields a reasonable amount of resolution without a large number of windings or a continuous system involving sliding contacts and their problems. The pyrex tube was then centered in a large copper pipe (the

inductance of the windings applies when they are in the pipe). This reduces noise pick-up and enables control of temperature. (see below).

After placing the two 200 μh windings in series with the transformer, the amount of capacitance necessary to achieve reactive balance was determined. For a capacitor in parallel with a resistor:

$$Z = \frac{R(1 - j\omega RC)}{1 + (\omega RC)^2} .$$

For reactive balance,

$$\omega \Delta L = \mathrm{Im}(Z)$$

where ΔL is the additional inductance required. Therefore,

$$\Delta L = \frac{-R_{s.g.}^2 C}{1 + (\omega R_{s.g.} C)^2}$$

where $R_{s.g.}$ is the resistance of a single strain gage. An amount of inductance close to that calculated was then added in series. For final precision balancing, a high resolution 50-1100 μμf air capacitor was used.

The chief disadvantage of this type of bridge is that the copper wire used in the windings of the inductor and the transformer has non-negligible resistance. Since copper has a large thermal coefficient of resistance, this type of bridge is temperature sensitive. For this reason, a system for controlling the temperature of critical components was built. These components are the strain gages, the two series decade

resistors, the inductor, the transformer, and the oscillator. All other elements carry very little current and have only a small effect on balance. Since it would be virtually impossible to control the temperature of lead wires and contacts, the former were made as short as possible using the heaviest gage available and the latter were good quality high frequency connectors.

Copper plates and pipes with copper tubing soft soldered to them were placed as close as possible to the critical components. The system for controlling temperature was constructed as in Fig. A.3. The water bath contains two copper coils (one for the system water and one for tap water), a mechanical stirrer, a heater, and a thermistor. The control temperature is set close to and slightly above room temperature. This makes control simple and radiative losses small. The cooling water is necessary to reject heat from the oscillator. The controller is an on-off type in which a thermistor controls a relay. The temperature of the water bath changes less than $0.1^{o}C$ over a period of several hours. To aid in maintaining constant temperature, all the copper parts surrounding the critical components are wrapped with fiber glass insulation.

The copper parts used in the temperature control system also help in shielding electronic components against noise. Where necessary, magnetic shielding foils were used as well. The main sources of pick-up were the transformer, ground loops, and loops in the bridge circuit. The foils were found to be highly effective in eliminating noise pick-up by the transformer. Judicious efforts were made to eliminate or

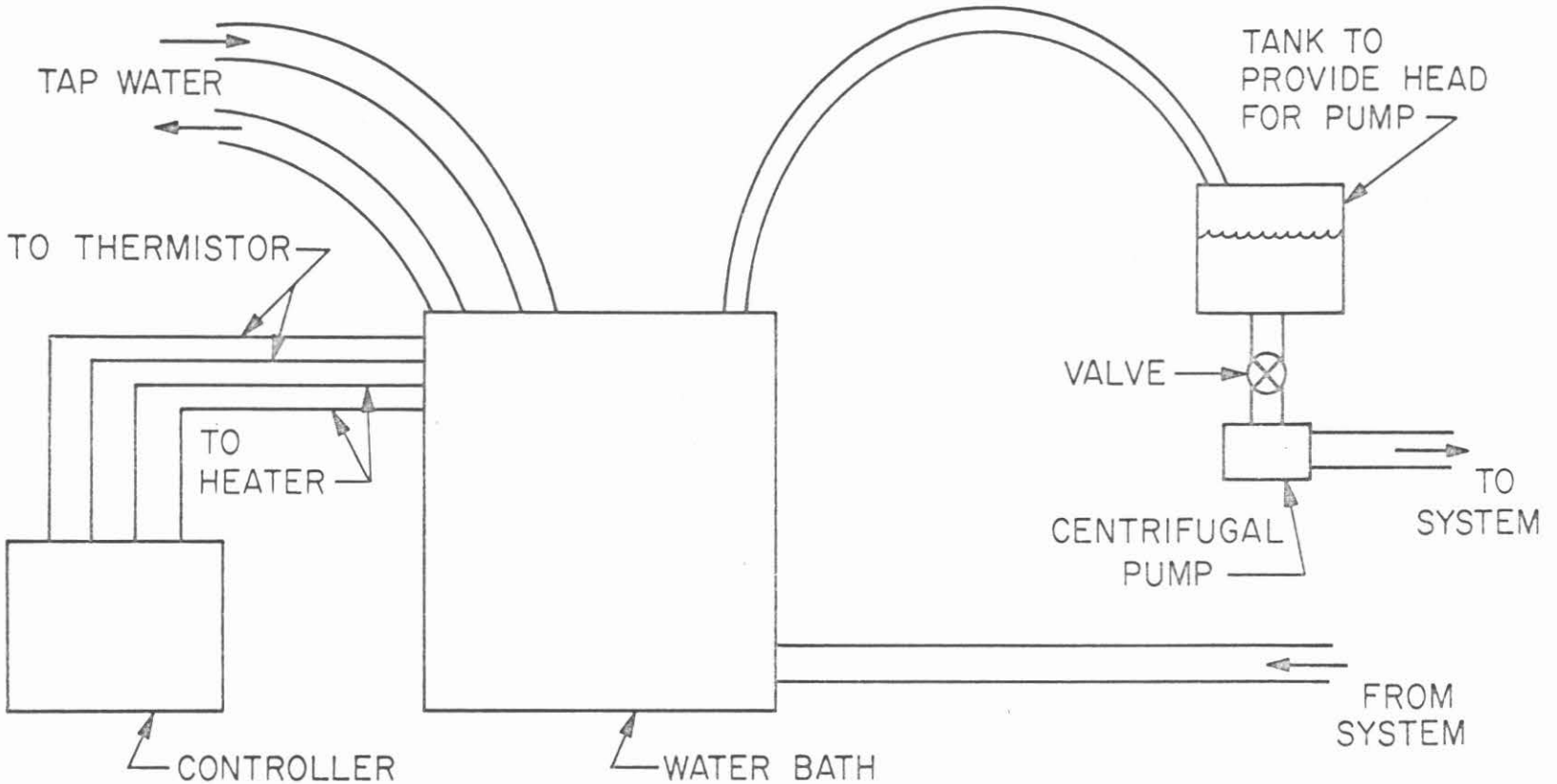

Fig. A.3. Diagram of the water system used to control the temperature of the strain gages and of the sensitive elements of the bridge (see Fig. A.2).

reduce the area of the two types of loops. Shielding foils were also used near right angle connectors. By these techniques it was possible to reduce the noise level observed on the lock-in amplifier well below the desired operating sensitivity.

The final bridge assembly is reasonably free of drift and noise. The capacitor used for fine balancing is virtually never changed, indicating excellent stability of reactive elements and negligible effect from any frequency drift. The balance point of the resistive elements changes in a fashion indicating that strain gage temperature control is not always too good. Since the strain gages are mounted on a very thin strip of phosphor bronze, the heat transfer is not sufficient. Futhermore they are subject to convection currents caused by cooling of the bottom of the pendulum. The latter can be eliminated by evacuating the chamber containing the pendulum. In this case the heat transfer to the copper pipe surrounding the strain gages is greatly reduced. From experience it was judged preferable to maintain a gas atmosphere at 10 to 15 lb/in^2 pressure in the chamber.

A possible improvement would be to have the bridge elements very close to the strain gages. These elements could consist of two wire-wound non-inductive resistors chosen so that only external balancing by means of variable parallel resistors is necessary. Another possibility is to have a longer phosphor bronze spring and four strain gages wired to double the output of the above system. A series resistor would be necessary to bring the bridge close to balance. Both of the above

arrangements would eliminate lead wire problems. If the strain gages were changed, balance could be restored merely by wiring in a single resistor of the appropriate value. Some form of temperature control would still be desirable but the bridge would be less temperature sensitive. However, the chief limiting factor in the entire system appears to be the non-zero magnetic moment of the pendulum coil. Measurements well into the range where this becomes significant can easily be made with the system as described.

A.3. Current Supply for the Pendulum Coil

The current is supplied by a Princeton Applied Research model TC-100.2BR Voltage/Current Reference Source. In the current mode, 0 to 100 milliamps are available and the resolution is several orders of magnitude better than required. Setting is done digitally and reaction time is very fast. Its digital setting feature eliminates the need for a separate potentiometer to measure current. The only drawback of digital setting is that a stepwise change in current imparts an impulse to the pendulum, affecting short term stability. However with experience and a rough idea of what the current should be, this is not a serious problem. The maximum current is fairly small. However, operation at a higher current could cause slight heating, causing erroneous temperature measurements. For materials with strong moments, it is better to reduce the mass than to use a large coil current.

A.4. Measurement and Control of Specimen Temperature

For the range 1.3°K to 4.2°K, the vapor pressure above condensed

helium (inside the specimen chamber) serves as an indication of temperature and a manostat (a pressure control device) maintains a set temperature. From 4.2°K to 77°K, the resistance of a germanium resistance thermometer indicates temperature and a balance between a small flow of liquid helium and a 0-4 watt heater is used for control. From 77°K to 300°K, a copper-constantan thermocouple indicates temperature and a balance between a small flow of liquid nitrogen and the heater is used for control.

Current to the Ge resistance thermometer is supplied by a 0-5 volt Kepco regulated power supply. It is operated in the voltage mode with a high resistance in series. (In the current mode, the minimum current is 1 ma which is too large.) Under these conditions, the current is very nearly independent of the resistance of the thermometer. The current is determined by measuring the voltage across a General Radio type 1441 100Ω standard resistor with a Leeds and Northrup type K Potentiometer. The voltage across the thermometer is also measured with the potentiometer and its resistance is thereby obtained. The temperature is found by comparison with a calibration made against another crystal whose calibration was supplied by the manufacturer.

All thermocouple wire connections are welded, and the leads are brought out of the dewar through glass-to-metal vacuum seals which enable a wire to pass through. The thermocouple voltage is measured with the type K potentiometer and compared with a reference table for for copper-constantan thermocouples. When it is known that the

measuring point is at the boiling point of nitrogen, the voltage reading is very close to the proper value and no additional calibration is necessary.

The heater consists of constantan wire wound around and attached to the copper wall of the specimen chamber. Its resistance is about 5 ohms. It was considered desirable to keep the lead wires small to avoid heat transfer, and the current is therefore limited to 900 ma. The heater current is supplied by an automatic temperature controller. Automatic temperature control is desirable for a number of reasons. First of all, it enables the operator to concentrate on making magnetic measurements without frequently having to check and adjust the temperature. Secondly, an automatic controller can reach a new set point without any attention from the operator. Finally, the more stable the temperature, the better the stability of the magnetometer. Since the effective thermal mass of the specimen chamber is both small and highly temperature dependent, proportional control as opposed to on-off control, rapid response and variable sensitivity to temperature fluctuations are necessary. A circuit diagram of the controller constructed is given in Fig. A.4. In operation, the thermocouple voltage is fed into a Cohu Kintel model 112A D.C. amplifier. The output is compared with an adjustable voltage (corresponding to the desired temperature). This difference voltage is then amplified and current is fed into the heater in proportion to this difference voltage. A nominal value of heater current may be set manually in order that the difference voltage be nearly zero at

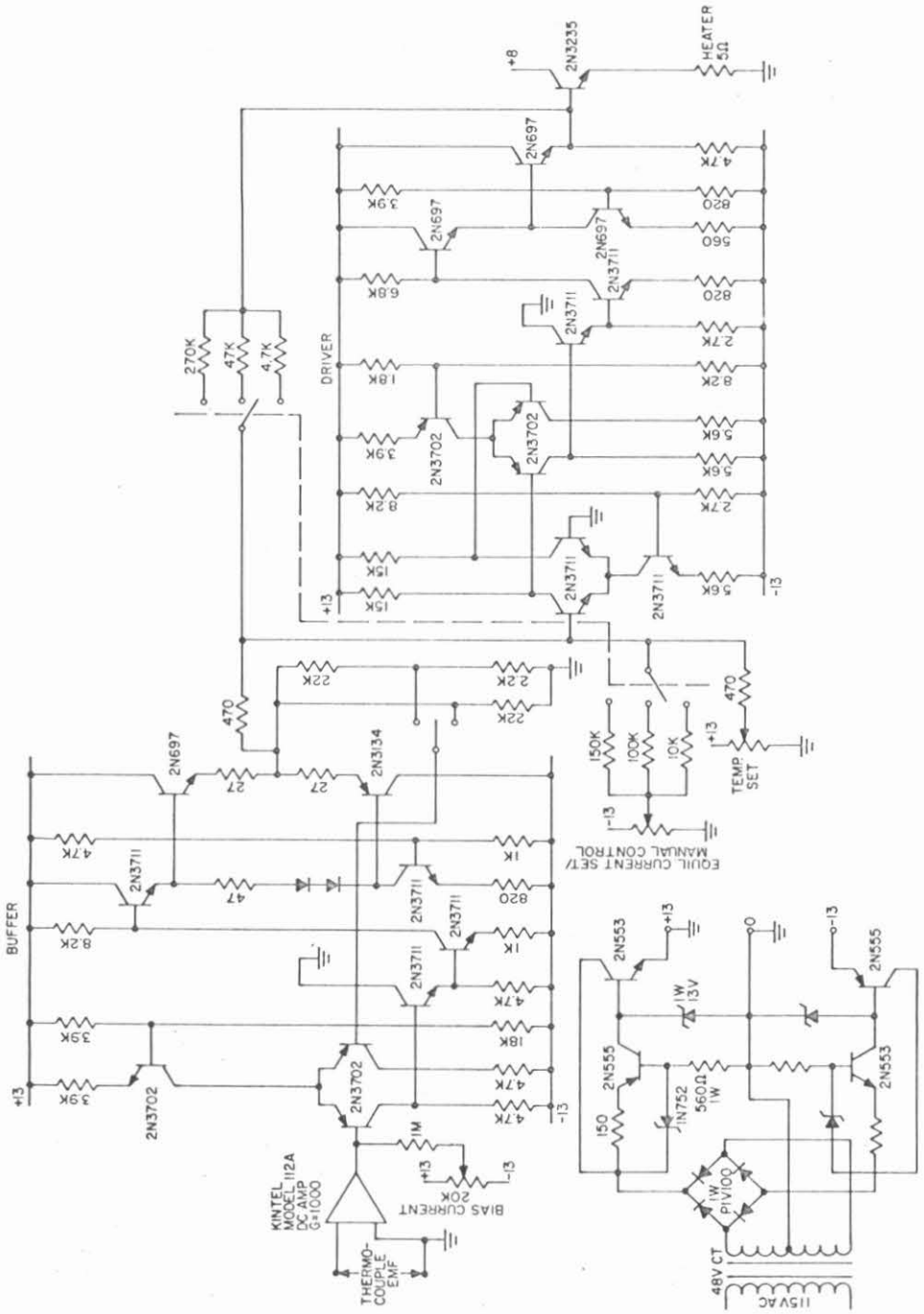

Fig. A.4. Diagram of the electrical circuit used for automatic control of the temperature of the specimen chamber.

the desired temperature. With experience, nearly critical damping and temperature control to better than $0.1^{o}C$ can be obtained.

REFERENCES

1. Charles O. Harris, Introduction to Stress Analysis, The Macmillan Company (1959), p. 97.

2. Harold Wayland, Differential Equations Applied in Science and Engineering, D. Van Nostrand Company, Inc. (1957), p. 70.